An update to this article is included at the end

Marine Geology 430 (2020) 106342

Contents lists available at ScienceDirect

Marine Geology

journal homepage: www.elsevier.com/locate/margo

Relative sea-level stability and the radiocarbon marine reservoir correction at Natuna Island, Indonesia, since 6400 yr BP

Jeannette Xiu Wen Wan[a,b,c,f,*], Aron J. Meltzner[a,b,*], Adam D. Switzer[a,b], Ke Lin[a], Xianfeng Wang[a,b], Sarah L. Bradley[d], Danny H. Natawidjaja[e], Bambang W. Suwargadi[e], Benjamin P. Horton[a,b]

[a] Earth Observatory of Singapore, Nanyang Technological University, 50 Nanyang Avenue, Singapore 639798, Singapore
[b] Asian School of the Environment, Nanyang Technological University, 50 Nanyang Avenue, Singapore 639798, Singapore
[c] CN Yang Scholars Programme, Nanyang Technological University, 50 Nanyang Avenue, Singapore 639798, Singapore
[d] Department of Geography, The University of Sheffield, Winter Street, Sheffield S3 7ND, United Kingdom
[e] Research Center for Geotechnology, Indonesian Institute of Sciences (LIPI), Kompleks LIPI, Gedung 70, Jalan Sangkuriang, Bandung, Jawa Barat 40135, Indonesia
[f] Department of Earth and Planetary Sciences, McGill University, 3450 University Street, Montreal, Quebec H3A 0E8, Canada

ARTICLE INFO

Keywords:
Holocene Relative Sea Level
Sunda Shelf
Coral Microatoll
Radiocarbon Marine Reservoir Correction

ABSTRACT

A high-precision relative sea level (RSL) record over the past 6400 years, reconstructed from fossil coral microatoll colonies, is reported for Natuna Island, Indonesia. The timing of 11 fossil microatolls from four sites on Natuna Island is constrained by replicate ^{14}C and ^{230}Th dates. We investigate the local marine reservoir correction (ΔR) using the replicate dates. The two sets of dates become aligned if a Marine20 ΔR of −143 ± 176 yr, 1σ (Marine13 ΔR of 15 ± 63 yr) is assigned to the ^{14}C dates. The distribution of microatoll ages and elevations indicates that RSL was relatively stable from 6400 to 1400 yr BP at 0.2–0.7 ± 0.4 m (2σ) higher than present, before a fall to current levels. A comparison with the predictions of a suite of glacial isostatic adjustment (GIA) models for Southeast Asia suggests refinements are needed in ice-history models to fully capture our RSL data. These new constraints on past RSL of the Sunda Shelf contribute to further calibration of GIA models in the tropics, where RSL data are presently insufficient.

1. Introduction

High-resolution reconstructions of Holocene relative sea level (RSL) are crucial to our understanding and forecasting of future sea-level conditions in response to modern climate change (e.g. Woodroffe and Murray-Wallace, 2012; Dutton et al., 2015; Khan et al., 2019). In Southeast Asia where hundreds of millions of people are at risk of anthropogenic sea-level rise, such reconstructions are important for applications such as capturing the natural background of sea-level variability in the region (e.g. Meltzner et al., 2017), and calibrating models of local to regional glacial isostatic adjustment (GIA) to constrain and predict the response to ice sheet change (e.g. Bradley et al., 2016; Tam et al., 2018). RSL change in Southeast Asia over the mid-to-late Holocene time period is of particular interest as its pattern is dominated by long-term GIA processes, particularly continental levering and equatorial ocean siphoning (Nakada and Lambeck, 1989; Mitrovica and Milne, 2002). High-resolution Holocene RSL records from the region, which have sufficient accuracy to characterise RSL variability, are critical to understanding these processes to model past and future ice-sheet and sea-level changes (Woodroffe and Horton, 2005; Lambeck et al., 2014).

RSL change since the Last Glacial Maximum (LGM) ~ 26 to 19 kyr BP has been spatially and temporally variable due to interactions between changes in ocean volume, isostatic effects, tectonics and redistribution of ocean water by climatological and oceanographic factors (Milne et al., 2009; Horton et al., 2018). A characteristic of mid-to-late Holocene RSL in tectonically stable far-field sites is a mid-Holocene highstand which characterizes the end of the dominant melting period during the LGM (e.g. Nakada and Lambeck, 1989; Baker and Haworth, 2000a, 2000b; Mitrovica and Milne, 2002; Lambeck et al., 2014). The magnitude and timing of this highstand provides an important constraint on geophysical models predicting sea level, as the highstand results from three globally applicable mechanisms affecting surface level and ocean volume: equatorial ocean siphoning, continental levering and ice melt (Nakada and Lambeck, 1989; Mitrovica and Milne, 2002). Previous studies on RSL of the Sunda Shelf loosely constrain the

* Corresponding authors.
E-mail addresses: jwan007@ntu.edu.sg (J.X.W. Wan), meltzner@ntu.edu.sg (A.J. Meltzner).

https://doi.org/10.1016/j.margeo.2020.106342
Received 10 October 2019; Received in revised form 2 September 2020; Accepted 14 September 2020
Available online 22 September 2020
0025-3227/ © 2020 The Authors. Published by Elsevier B.V. This is an open access article under the CC BY license (http://creativecommons.org/licenses/by/4.0/).

timing of this highstand from 7000 to 4000 yr BP, and between +1 m to up to +5 m in magnitude (Geyh et al., 1979; Horton et al., 2005; Bird et al., 2010; Meltzner et al., 2017). This variation in magnitude is proposed to be due to spatial variability in hydro-isostatic effects (Horton et al., 2005). Details of the highstand however remain poorly constrained on the Sunda Shelf (Yu et al., 2009), in part due to the low resolution RSL indicators (Horton et al., 2005) or as a result of variations caused by the irregular shape of coastlines and local processes (Zong, 2004).

There is variability on the subsequent trend of far-field RSL fall since the mid-Holocene reported along both the Sunda Shelf (Khan et al., 2015) and the Australian coast (Lewis et al., 2013). On the Sunda Shelf, RSL fall may have exhibited oscillatory behavior (Geyh et al., 1979; Bird et al., 2010; Tam et al., 2018; Mann et al., 2019). Extensive studies of proxy RSL data on the tectonically stable, far-field Australian coast suggests that there are three main possibilities: a smoothly falling RSL since the mid-Holocene highstand, a stable mid-to-late Holocene highstand followed by a fall in more recent times, and an oscillating mid-to-late Holocene RSL (Baker and Haworth, 2000a, 2000b; Sloss et al., 2007; Perry and Smithers, 2011; Leonard et al., 2016). The high-resolution data contributed from this study can help to inform us on this variability in mid-Holocene RSL behavior on the Sunda Shelf.

Coral microatolls are one of the high-resolution RSL indicators due to their narrow living range near the sea-level surface (Smithers and Woodroffe, 2000; Hibbert et al., 2016) and present a good opportunity to overcome the lack of abundant and high-resolution RSL records in the Sunda Shelf (Woodroffe and Horton, 2005; Lambeck et al., 2014). We have derived a proxy record of mid-to-late Holocene RSL from coral microatoll colonies off the eastern coast of Natuna Island, Indonesia (Fig. 1) (Section 3.2). Sea-level index points were obtained from a detailed survey of the elevations of the fossil microatolls combined with cores drilled vertically, downward from the upper surface of the microatoll, for both ^{14}C and ^{230}Th dating. Results indicate that RSL was relatively stable from 6400 to 1400 yr before present (BP, where the present is defined as the year 1950 CE) at 0.2–0.7 ± 0.4 m (2σ) higher than present, before a more recent fall to current levels with no evidence of oscillations. We also compare results between ^{14}C and ^{230}Th dates of coeval samples, which show consistency with a marine calibration correction value of Marine20 $\Delta R = -143 \pm 176$ yr, 1σ (Marine13 $\Delta R = 15 \pm 63$ yr) for the sites.

2. Study site

Natuna Island, Indonesia (3.9°N 108.2°E), is located in the South China Sea between northwestern Borneo and eastern Peninsular Malaysia, within a region of the Sunda Shelf inferred to be tectonically stable based on analysis of ten years of GPS velocities (Simons et al., 2007) (Fig. 1). The only earthquakes exceeding magnitude 4.0 recorded within 400 km of Natuna Islands were an m_b 4.3 event in August 2001, 190 km northwest of Natuna, and an m_b 4.7 event in August 2011, 330 km south of Natuna, though the earthquake catalog would have been complete only at higher magnitudes farther back in time (ANSS Comprehensive Earthquake Catalog (ComCat), https://earthquake.usgs.gov/earthquakes/search/). Just east of Natuna, in the southern part of the East Natuna Basin, Pliocene faults are common, but there is a general lack of evidence for activity along those faults since the Pleistocene (Wirojudo and Wongsosantiko, 1985). However, inferred displacement in the past ~7000 years along a possibly reactivated fault ~230 km southeast of Natuna (Majewski et al., 2018) raises questions about the inferred tectonic stability of the region, and an enigmatic and poorly located but widely felt earthquake in June 1874, perhaps as little as ~400 km to the southwest in the Karimata Strait (Martin et al., 2020), reminds us how poorly understood the recent tectonics of this region actually are.

In the long term, the region may be slowly subsiding. Parham (2016, 2019) surveyed much of the Peninsula Malaysia and Malaysian Borneo coastlines and argued, based on an absence of pre-Holocene RSL indicators above present sea level in the "Sundaland" portion of Malaysia (Fig. 1), that this region is subsiding on 10^4 to 10^6 yr timescales. Likewise, Sarr et al. (2019) proposed that reefs narrower than 10 km only developed in the Quaternary where a region is subsiding, and where the subsidence rates have exceeded 0.2 mm/yr on average; because reefs on the Sunda Shelf are generally narrower than 10 km, they argued that the entire Sunda Shelf, including Natuna Island, has been subsiding since the Pleistocene. In the Holocene, this would represent a small portion of RSL change due to ice melting and GIA.

Fossil coral microatolls are abundant along the northeastern coast of Natuna. We reconstruct RSL using microatolls from four sites which are within 22 km of one another: PNTN-A, B, C and D (Fig. 1).

The ~2.0 m tidal range at Natuna Island is modulated by the 18.6-year nodal tidal cycle, such that, over the 18.6-year cycle, there is a ~0.2 m variation in the lowest predicted tides of the year (Fig. 2). Microatoll morphology is controlled by extreme low water level, and we expect die-downs to occur during periods of this cycle when annual lowest tide is getting progressively lower, or is at its lowest levels (Meltzner et al., 2017). From tidal model predictions, the most recent die-downs experienced by modern microatolls on Natuna Island should have occurred in the interval between 2001 and 2006. As the 18.6-year cycle is likely to have modulated the tides in a similar manner during the lifetimes of the fossil microatolls in the study, we expect a similar periodicity in the die-downs and morphology of fossil microatoll annuli.

3. Methods

3.1. Chronological analysis

3.1.1. Dating analysis and associated temporal uncertainties

To determine the age of our RSL indicators a minimum of two ^{14}C dates (Table 1) and one ^{230}Th date (Table 2) was obtained for each fossil microatoll core. ^{230}Th dating samples were obtained ~2 cm below the corresponding ^{14}C dating samples in each core. As a result, ^{230}Th samples are estimated to be 3 ± 4 years older than the corresponding ^{14}C samples. ^{14}C and ^{230}Th dating results are compared in Table 3. Further details on sample preparation and measurement methods can be found in Appendix A. High-precision ^{230}Th ages are used as an independent chronometer to compare with calibrated ^{14}C dates to obtain the marine reservoir correction value, ΔR, for Natuna Island.

3.1.2. Radiocarbon marine reservoir correction (ΔR) for Natuna Island

^{14}C analysis is useful for dating Holocene and latest Pleistocene samples from a variety of materials. However, due to temporal fluctuation in atmospheric ^{14}C and spatial variation of ^{14}C distribution in natural reservoirs, ^{14}C dates must undergo calibration with respect to an independent chronometer (Stuiver et al., 1986; Cutler et al., 2004; Reimer et al., 2013b). Furthermore, marine samples require a marine reservoir correction, ΔR. This correction varies by location (and possibly over time) and must be independently obtained for each location (Stuiver et al., 1986; Alves et al., 2018).

We adopt the method of estimating ΔR using high-precision ^{230}Th dating as an independent chronometer representing the known age of a sample for ^{14}C calibration (Cao et al., 2007; McGregor et al., 2008). ΔR values were calculated from paired ^{14}C and ^{230}Th dates on each coral sample using the online program *deltar* (Reimer and Reimer, 2017) based on Soulet (2015). ΔR was calculated both for the older calibration curves (Marine13 and earlier; Hughen et al., 2004; Reimer et al., 2009, 2013a; http://calib.org/deltar13/) and for the new calibration curve (Marine20; Heaton et al., 2020; http://calib.org/deltar/) (Table 4).

For samples with duplicate ^{14}C or duplicate ^{230}Th dates, the weighted mean ($\bar{x}$; Eq. 1) and scale-corrected standard error of the weighted mean ($\hat{\sigma}_{\bar{x}}$; Eq. 2) of the duplicate conventional ^{14}C ages or the duplicate ^{230}Th ages were first calculated as

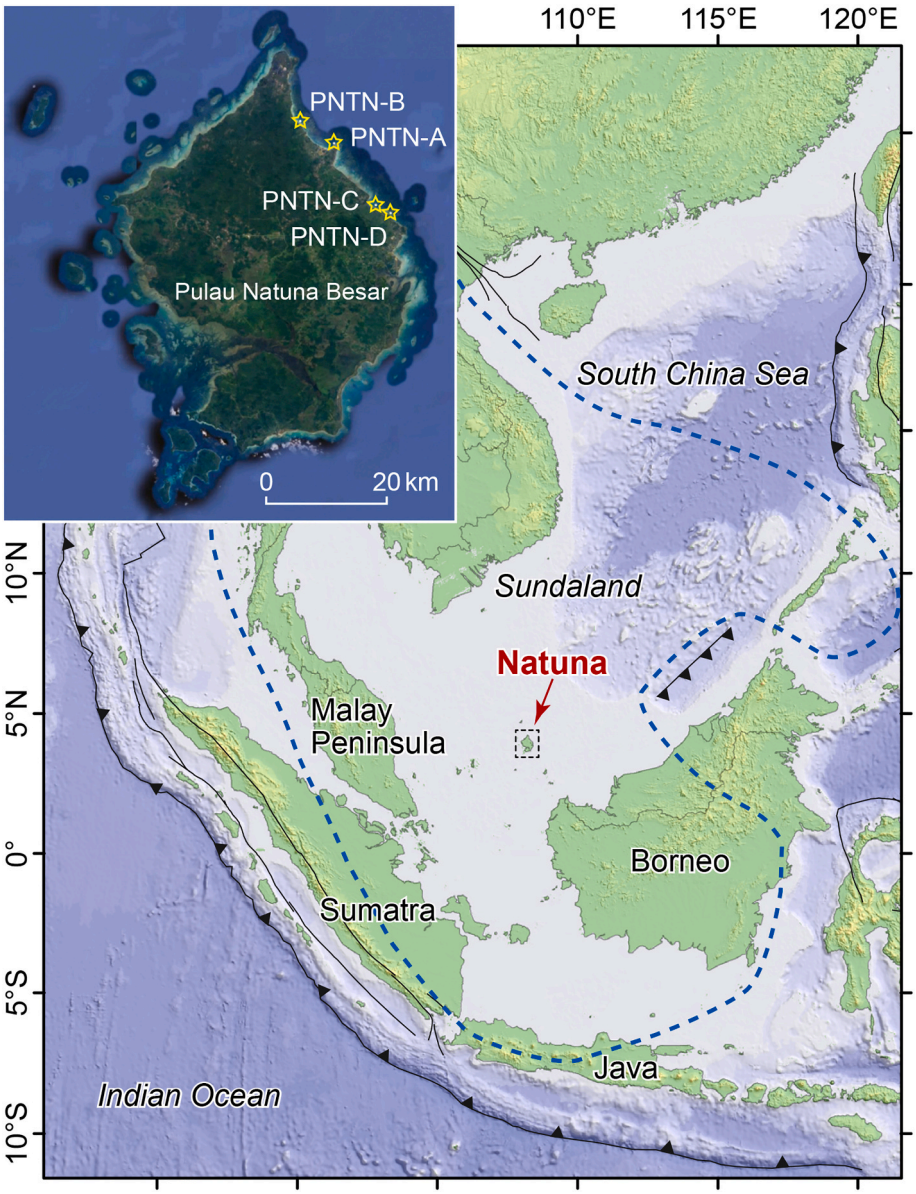

Fig. 1. Map showing Natuna Island and the tectonically stable Sundaland block. Blue dashed line contains the region where land is currently deforming internally at rates less than 4 mm/yr (Simons et al., 2007). Solid black lines are primary fault traces; barbed lines are mapped or inferred subduction zones. The inset shows the four study sites (PNTN-A,B,C,D) on Pulau Natuna Besar (Big Natuna Island); the location of the inset is shown on the main map with a dashed box. The distance between PNTN-B and PNTN-D is ~22 km. (For interpretation of the references to colour in this figure legend, the reader is referred to the web version of this article.)

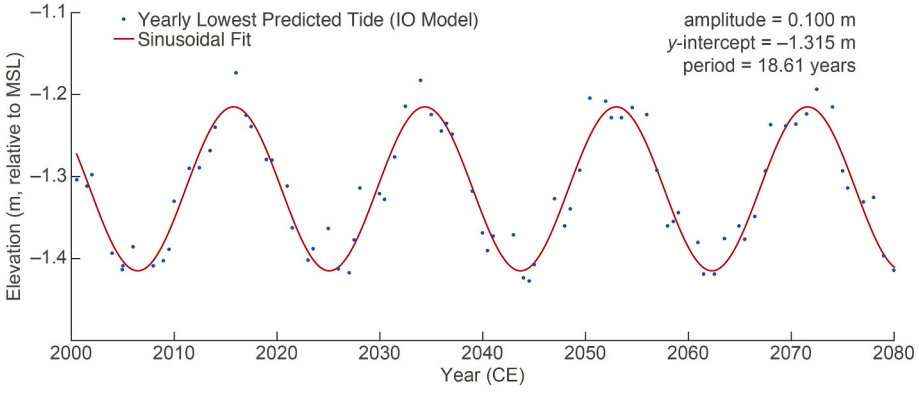

Fig. 2. The predicted lowest tide of each year, from the Oregon State University regional tidal model for the Indian Ocean (IO) region (Egbert and Erofeeva, 2002), for site PNTN-A on Natuna Island. The yearly lowest tides are fit by a sinusoid with 18.61-year periodicity and a double amplitude of 20 cm. Details of the tide model are in Appendix D.

Table 1
^{14}C dates of *Porites* fossil microatolls on Natuna Island.

Site/ Sample ID	Rafter ID	δ^{13}C (± error)[1] (‰)			^{14}C Age ± 1σ[2] (rcy BP)[3]		
PNTN-A							
A-F1	40,883/7	−1.3	±	0.2	1888	±	27
	40,883/7	−2.4	±	0.2	1859	±	26
A-F2	40,998/1	−1.1	±	0.2	5930	±	28
	40,998/1	−1.2	±	0.2	5914	±	29
A-F3	40,998/2	−1.3	±	0.2	5360	±	28
	40,998/2	−2.0	±	0.2	5368	±	29
A-F4A	40,883/8	−0.9	±	0.2	5706	±	42
	40,883/8	−1.0	±	0.2	5772	±	29
A-F4B	40,998/3	−0.2	±	0.2	5902	±	28
	40,998/3	−0.1	±	0.2	5925	±	28
PNTN-B							
B-F1	40,883/6	−1.5	±	0.2	2335	±	27
	40,883/6	−1.2	±	0.2	2348	±	26
B-F2	40,998/4	−0.3	±	0.2	2153	±	25
	40,998/4	−1.3	±	0.2	2229	±	26
B-F3	40,998/5	−0.6	±	0.2	2113	±	25
	40,998/5	−1.5	±	0.2	2132	±	26
PNTN-C							
C-F1	40,883/9	−1.5	±	0.2	3145	±	40
	40,883/9	−1.3	±	0.2	3229	±	27
C-F2	40,998/6	−2.1	±	0.2	2598	±	25
	40,998/6	−1.8	±	0.2	2561	±	26
PNTN-D							
D-F1	40,883/10	−3.2	±	0.2	3451	±	40
	40,883/10	−3.5	±	0.2	3495	±	27
D-F2	40,998/7	−2.0	±	0.2	4457	±	27
	40,998/7	−2.4	±	0.2	4530	±	28

[1] We report the environmental (pre-fractionation) δ^{13}C measured offline by IRMS. This value is not used in ^{14}C age calculations.

[2] Conventional radiocarbon ages are from Rafter Radiocarbon Laboratory, GNS Science, and are reported as defined by Stuiver and Polach (1977). The reported errors comprise statistical errors in sample and standard determinations, combined in quadrature with a system error component based on the analysis of an ongoing series of measurements on an oxalic acid standard. Further analysis details are available on request.

[3] rcy BP is "radiocarbon years before present", where the "present" is defined as the year 1950 CE.

$$\bar{x} = \frac{\sum_{i=1}^{n} x_i\, \sigma_i^{-2}}{\sum_{i=1}^{n} \sigma_i^{-2}} \tag{1}$$

$$\hat{\sigma}_{\bar{x}} = \sqrt{\frac{1}{\sum_{i=1}^{n} \sigma_i^{-2}} \times \frac{1}{n-1} \sum_{i=1}^{n} \frac{(x_i - \bar{x})^2}{\sigma_i^2}} \tag{2}$$

where x_i is the measurement, σ_i is the error of measurement, and n is the number of measurements. $\hat{\sigma}_{\bar{x}}$ estimates the error associated with the mean of multiple independent measurements of a quantity and includes a reduced-χ^2 term to correct for unaccounted sources of error in each dating result.

An alternative method for calculating the standard error of the weighted mean does not involve a correction for over- or under-dispersion, but is commonly applied in studies involving ^{230}Th dating techniques (e.g., Sieh et al., 2008; Chiang et al., 2019). We find that repeating the calculation using the uncorrected standard error of the weighted mean ($\sigma_{\bar{x}}$) produces a similar ΔR estimate (Appendix B).

For an overall population estimate of ΔR, the weighted mean ($\bar{x}$) and weighted standard deviation ($\hat{\sigma}$; Eq. 3) of all *deltar* results were calculated, with

$$\hat{\sigma} = \sqrt{\frac{1}{\sum_{i=1}^{n} \sigma_i^{-2}} \times \frac{n}{n-1} \sum_{i=1}^{n} \frac{(x_i - \bar{x})^2}{\sigma_i^2}} \tag{3}$$

Separately, we also estimated ΔR for each sample, and a joint ΔR for all the samples, using the Bayesian methodologies of OxCal (Bronk Ramsey, 2009). Details are in Appendix C and Table A2. The results from OxCal are comparable to those determined using *deltar*.

3.2. Elevation analysis: reconstructing high-resolution paleo-RSL using coral microatolls

Coral microatolls are large circular colonies of coral that survive near low water in marine intertidal zones in the tropics, and which have a characteristic concentric ring morphology on their upper surface (Scoffin and Stoddart, 1978). They can serve as high-precision RSL indicators as their morphologies reflect RSL changes during coral growth (Meltzner et al., 2017). Subaerial exposure during periods of lower RSL kills the upper surface of the coral, restricting vertical growth whilst horizontal growth along the submerged margin remains unaffected (Meltzner and Woodroffe, 2015). When a coral's vertical growth is constrained, it is evident in unconformities in microatoll morphology, termed a coral "die-down". Characteristic of many microatolls is a morphology of concentric ridges (annuli) on an otherwise flat upper surface (Fig. 3; Supplementary Figs. S1–S11). This arises when a coral colony experiences multiple die-down events, whilst continuing to grow below its highest level of survival (HLS). We can use corals to track RSL, as the vertical elevation of die-downs gives a precise indication of RSL at that point in time (Yu et al., 2009). In the absence of die-downs, the vertical elevation due to coral growth provides a minimum limiting estimate of RSL when the coral was alive.

Below sea level, the highest level of growth (HLG) of a coral is determined by the coral growth rate, and provides a minimum bound on RSL in any year (Meltzner and Woodroffe, 2015). A microatoll colony's average lifetime spans decades, with over two centuries of RSL history recorded for the largest colonies (e.g., Philibosian et al., 2014; Meltzner et al., 2017). Radiometric dating allows for the age of the colony to be established and piecing together records from numerous samples allows us to generate an indicative RSL history map over a sustained time period.

A sea-level index point estimates RSL at a specified time and place, with an associated uncertainty (Shennan et al., 2015). In contrast, minimum limiting data provide only a minimum bound on RSL at a particular time and place (Shennan and Horton, 2002). In this study, points surveyed along the crests of sequential concentric annuli on the surface of a microatoll are HLG data, and therefore minimum limiting data on RSL. However, the very existence of the concentric annuli informs us that a sequence of die-downs (HLS data) occurred near the upper surface of the microatoll. Therefore, the surveyed elevations of the concentric annuli are necessarily close to RSL, and with sufficiently large errors we can also treat such data as sea-level index points.

To produce sea-level index points from microatoll elevation data, the indicative meaning of the proxy indicator must be established (van de Plassche, 1986). It is defined as the relationship between the sample to a contemporaneous reference water level, with an associated error known as the indicative range (Shennan, 1986; van de Plassche, 1986; Horton et al., 2000). Determining this relationship between the sample and the local tidal level when formed allows us to easily put all sea-level proxy data into a common datum. The indicative meaning of a sea-level index point involves two parameters: (1) the reference water level, which is the modern elevation at which the indicator occurs, and (2) the indicative range, which is the modern vertical range the indicator occurs at (van de Plassche, 1986). In the subsequent sections, we provide details on our methods to produce paleo-RSL data from fossil coral microatolls in Natuna Island.

3.2.1. Fitting surveyed elevations to a common tidal datum

In order to combine our observations from fossil *Porites* microatolls at four sites to reconstruct past RSL at Natuna, we must place all elevations into a common datum. The most straightforward means to accomplish this would be to use living *Porites* HLS at each site as the reference elevation for the site: the difference between fossil and living

Table 2
^{230}Th dates of *Porites* fossil microatolls on Natuna Island.

Site/Sample	^{238}U		^{232}Th		δ^{234}U measured[1]		[^{230}Th/^{238}U][2]		[^{230}Th/^{232}Th][3]	^{230}Th Age (uncorrected)		^{230}Th Age (corrected)[4,5]		$\delta^{234}U_{initial}$ corrected[6]		^{230}Th Age (corrected, in yr BP)[7]			
ID	(ppb)		(ppt)		(‰)		(activity)		($\times 10^{-6}$)	(yr)		(yr)		(‰)		(individual dates)		(weighted mean)	
PNTN-A																			
A-F1	2360	± 2	2811	± 56	144.3	± 1.3	0.0159	± 0.0001	220 ± 5	1524.8	± 7.9	1494.5	± 22.8	144.9	± 1.3	1427.5	± 22.8	1419.3	± 8.2
	2361	± 3	2784	± 56	145.1	± 1.6	0.0157	± 0.0001	220 ± 5	1508.1	± 8.4	1478.1	± 22.8	145.7	± 1.6	1411.1	± 22.8		
A-F2	2480	± 5	192	± 5	143.5	± 2.0	0.0637	± 0.0002	13,547 ± 362	6241.7	± 23.7	6239.7	± 23.7	146.0	± 2.0	6172.7	± 23.7	6182.9	± 9.5
	2478	± 3	193	± 5	142.1	± 1.5	0.0638	± 0.0002	13,488 ± 359	6260.7	± 22.0	6258.7	± 22.0	144.6	± 1.5	6191.7	± 22.0		
A-F3	2280	± 3	242	± 7	144.7	± 1.6	0.0596	± 0.0002	9248 ± 265	5826.0	± 18.9	5823.3	± 18.9	147.1	± 1.6	5756.3	± 18.9	5756.3	± 18.9
A-F4A	2425	± 3	3198	± 64	143.9	± 1.5	0.0642	± 0.0002	803 ± 16	6290.2	± 19.8	6256.7	± 30.9	146.5	± 1.5	6189.7	± 30.9	6177.9	± 8.6
	2427	± 4	1236	± 25	142.9	± 1.8	0.0637	± 0.0002	2064 ± 42	6251.5	± 20.7	6238.6	± 22.6	145.4	± 1.8	6171.6	± 22.6		
A-F4B	2471	± 3	927	± 19	143.5	± 1.4	0.0655	± 0.0002	2876 ± 59	6420.5	± 21.5	6411.0	± 22.5	146.1	± 1.4	6344.0	± 22.5	6338.7	± 5.3
	2469	± 4	940	± 19	142.8	± 1.7	0.0653	± 0.0002	2829 ± 58	6410.0	± 21.5	6400.4	± 22.6	145.4	± 1.7	6333.4	± 22.6		
PNTN-B																			
B-F1	1978	± 3	142	± 5	145.9	± 1.8	0.0208	± 0.0001	4771 ± 172	2000.8	± 9.2	1999.0	± 9.3	146.7	± 1.8	1932.0	± 9.3	1932.0	± 9.3
B-F2	2137	± 2	186	± 8	145.0	± 1.6	0.0192	± 0.0001	3647 ± 152	1845.3	± 11.8	1843.1	± 11.9	145.8	± 1.6	1776.1	± 11.9	1776.1	± 11.9
B-F3	2457	± 4	164	± 6	143.4	± 1.8	0.0186	± 0.0001	4584 ± 172	1783.0	± 9.1	1781.3	± 9.2	144.2	± 1.8	1714.3	± 9.2	1714.3	± 9.2
PNTN-C																			
C-F1	2171	± 3	123	± 6	144.5	± 1.8	0.0313	± 0.0001	9131 ± 431	3021.6	± 12.9	3020.1	± 12.9	145.8	± 1.8	2953.1	± 12.9	2953.1	± 12.9
C-F2	2267	± 3	45	± 8	144.0	± 1.6	0.0243	± 0.0001	20,058 ± 3333	2344.5	± 12.5	2344.0	± 12.6	145.0	± 1.6	2277.0	± 12.6	2277.0	± 12.6
PNTN-D																			
D-F1	2052	± 2	742	± 16	146.0	± 1.5	0.0356	± 0.0001	1625 ± 35	3443.0	± 14.4	3433.8	± 15.8	147.4	± 1.5	3366.8	± 15.8	3366.8	± 15.8
D-F2	2408	± 4	2452	± 49	142.7	± 1.6	0.0492	± 0.0002	797 ± 16	4797.9	± 17.7	4772.0	± 25.5	144.6	± 1.6	4705.0	± 25.5	4696.5	± 8.9
	2408	± 4	2376	± 48	142.8	± 1.7	0.0490	± 0.0002	820 ± 17	4779.4	± 19.6	4754.3	± 26.4	144.7	± 1.8	4687.3	± 26.4		

Analytical errors are 2σ of the mean.

[1] $\delta^{234}U = ([^{234}U/^{238}U]_{activity} - 1) \times 1000$.

[2] $[^{230}Th/^{238}U]_{activity} = 1 - e^{-\lambda_{230}T} + (\delta^{234}U_{measured}/1000)[\lambda_{230}/(\lambda_{230} - \lambda_{234})](1 - e^{-(\lambda_{230} - \lambda_{234})T})$, where T is the age. U decay constants: $\lambda_{238} = 1.55125 \times 10^{-10}\,yr^{-1}$ (Jaffey et al., 1971) and $\lambda_{234} = 2.82206 \times 10^{-6}\,yr^{-1}$ (Cheng et al., 2013). Th decay constant: $\lambda_{230} = 9.1705 \times 10^{-6}\,yr^{-1}$ (Cheng et al., 2013).

[3] The degree of detrital ^{230}Th contamination is indicated by the ^{230}Th/^{232}Th atomic ratio instead of the activity ratio.

[4] Corrected ^{230}Th ages assume the initial ^{230}Th/^{232}Th atomic ratio of $4.4 \pm 2.2 \times 10^{-6}$. Those are the values for a material at secular equilibrium, with the bulk earth ^{232}Th/^{238}U value of 3.8. The errors are arbitrarily assumed to be 50%.

[5] The ^{230}Th-dating chemistry and measurements were performed in mid-2017.

[6] $\delta^{234}U_{initial}$ (corrected) was calculated based on ^{230}Th age (T), i.e., $\delta^{234}U_{initial} = \delta^{234}U_{measured} \times e^{\lambda_{234}T}$, and T is corrected age.

[7] BP stands for "Before Present" where the "present" is defined as the year 1950 CE.

Table 3
Summary of ^{230}Th and ^{14}C dating results.

Site/Sample ID	Corrected ^{230}Th Age (yr BP) ± 2σ[1]						Conventional ^{14}C Age (rcy BP) ± 1σ[1,2]			
	Individual dates		Weighted mean		Weighted mean offset by − 3 ± 4 yr[3,4]		Individual dates		Weighted mean[4]	
PNTN-A										
A-F1	1427.5	± 22.8	1419.3	± 8.2	**1416.3**	**± 9.1**	1888	± 27	**1873.0**	**± 14.5**
	1411.1	± 22.8					1859	± 26		
A-F2	6172.7	± 23.7	6182.9	± 9.5	**6179.9**	**± 10.3**	5930	± 28	**5922.3**	**± 8.0**
	6191.7	± 22.0					5914	± 29		
A-F3	5756.3	± 18.9	5756.3	± 18.9	**5753.3**	**± 19.4**	5360	± 28	**5363.9**	**± 4.0**
							5368	± 29		
A-F4A	6189.7	± 30.9	6177.9	± 8.6	**6174.9**	**± 9.5**	5706	± 42	**5750.7**	**± 30.9**
	6171.6	± 22.6					5772	± 29		
A-F4B	6344.0	± 22.5	6338.7	± 5.3	**6335.7**	**± 6.6**	5902	± 28	**5913.5**	**± 11.5**
	6333.4	± 22.6					5925	± 28		
PNTN-B										
B-F1	1932.0	± 9.3	1932.0	± 9.3	**1929.0**	**± 10.1**	2335	± 27	**2341.7**	**± 6.5**
							2348	± 26		
B-F2	1776.1	± 11.9	1776.1	± 11.9	**1773.1**	**± 12.5**	2153	± 25	**2189.5**	**± 38.0**
							2229	± 26		
B-F3	1714.3	± 9.2	1714.3	± 9.2	**1711.3**	**± 10.0**	2113	± 25	**2122.1**	**± 9.5**
							2132	± 26		
PNTN-C										
C-F1	2953.1	± 12.9	2953.1	± 12.9	**2950.1**	**± 13.5**	3145	± 40	**3202.7**	**± 39.0**
							3229	± 27		
C-F2	2277.0	± 12.6	2277.0	± 12.6	**2274.0**	**± 13.2**	2598	± 25	**2580.2**	**± 18.5**
							2561	± 26		
PNTN-D										
D-F1	3366.8	± 15.8	3366.8	± 15.8	**3363.8**	**± 16.3**	3451	± 40	**3481.2**	**± 20.4**
							3495	± 27		
D-F2	4705.0	± 25.5	4696.5	± 8.9	**4693.5**	**± 9.7**	4457	± 27	**4492.2**	**± 36.5**
	4687.3	± 26.4					4530	± 28		

[1] BP is "before present" where the "present" is defined as the year 1950 CE.
[2] rcy is "radiocarbon years".
[3] We estimate ^{230}Th samples to be systematically 3 ± 4 years older than corresponding ^{14}C samples, based on the samples' positions in the cores. We adjust the ^{230}Th sample ages by this amount so that the comparison between ^{230}Th and ^{14}C ages would occur on material of exactly the same age. The 2σ errors of the ^{230}Th age and the offset are combined in quadrature.
[4] Ages in bold are used for ΔR estimates (Table 4).

Table 4
ΔR calculation for Natuna Island (*deltar* results).

Site/Sample ID	^{14}C Age (rcy BP) ± 1σ[1,2,3]		Offset ^{230}Th Age (yr BP) ± 1σ[1,3,4]		ΔR (yr) ± 1σ[4] *deltar* result			
	(weighted mean)		(weighted mean)		for Marine13		for Marine20	
PNTN-A								
A-F1	1873.0	± 14.5	1416.3	± 4.6	−16	± 15	−165	± 31
A-F2	5922.3	± 8.0	6179.9	± 5.1	172	± 12	−19	± 23
A-F3	5363.9	± 4.0	5753.3	± 9.7	−38	± 10	−210	± 21
A-F4A	5750.7	± 30.9	6174.9	± 4.8	10	± 32	−183	± 64
A-F4B	5913.5	± 11.5	6335.7	± 3.3	−20	± 12	−206	± 24
PNTN-B								
B-F1	2341.7	± 6.5	1929.0	± 5.1	22	± 8	−118	± 17
B-F2	2189.5	± 38.0	1773.1	± 6.3	18	± 38	−144	± 77
B-F3	2122.1	± 9.5	1711.3	± 5.0	−10	± 10	−161	± 23
PNTN-C								
C-F1	3202.7	± 39.0	2950.1	± 6.8	36	± 40	−96	± 79
C-F2	2580.2	± 18.5	2274.0	± 6.6	20	± 20	−128	± 40
PNTN-D								
D-F1	3481.2	± 20.4	3363.8	± 8.2	−3	± 23	−144	± 45
D-F2	4492.2	± 36.5	4693.5	± 4.9	2	± 36	−155	± 74

[1] BP is "before present" where the "present" is defined as the year 1950 CE.
[2] rcy is "radiocarbon years".
[3] Values are from Table 3.
[4] ΔR estimates calculated using the *deltar* programme: http://calib.org/deltar13/ for Marine13 and http://calib.org/deltar/ for Marine20. *deltar* requires all uncertainties to be input as 1σ errors (P. Reimer, personal communication, 2017), so we have halved the 2σ ^{230}Th age errors from Table 3.

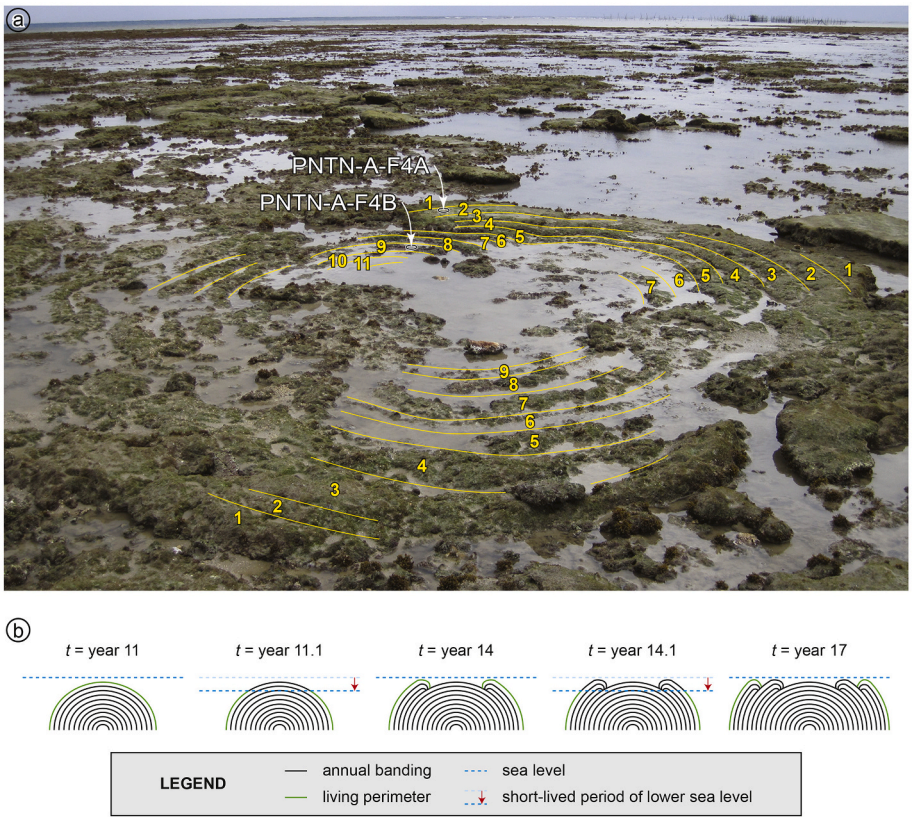

Fig. 3. Fossil microatoll colony PNTN-A-F4 from site PNTN-A on Natuna Island, Indonesia, with a schematic cross section of the formation of a microatoll ring morphology. The radius of PNTN-A-F4 is ~2.7 m, which is the average distance between the centre and outer ring of the microatoll from surveyed points. **(a)** PNTN-A-F4 has at least thirteen concentric rings around a central low. Rings are traced where clearly identifiable in the photo, but the two innermost rings are obscured by water; some rings were more apparent when viewed from other angles. Rings are counted inward from the outside. Sample cores PNTN-A-F4A and PNTN-A-F4B are located with white arrows. **(b)** A possible chronology showing how short-term fluctuations in RSL (at t = 11.1 and 14.1 years) can contribute to the formation of concentric rings, even in the absence of long-term RSL change (modified from Meltzner and Woodroffe, 2015).

Porites HLS would be interpreted as the RSL change over that time period (Woodroffe and Barlow, 2015; Meltzner et al., 2017). However, we did not find abundant living microatolls at all sites (no living microatolls were found at site PNTN-B), and where they were found, we could not always refute the possibility that the living microatolls were growing in isolated ponds on the reef flat, higher than the HLS of similar microatolls in the open ocean.

To circumvent this problem, we define a common tidal datum. Meltzner et al. (2010) argued that the HLS of *Porites* corals closely tracks the lowest water level each year. To compare microatoll elevations across the four sites (PNTN-A, B, C and D), we used the lowest tide at each site in 2012 as the common datum:

$$\text{HLG (or HLS)} = \text{surveyed elevation of microatoll ring} - \text{lowest tide in 2012 CE} \quad (4)$$

To calculate the elevation of the lowest tide at each site in 2012 (the year of field work), we repeatedly surveyed open-ocean water level, noting the exact time of each water-level measurement, while visiting the site to sample and survey the elevations of microatolls. We then compared the surveyed water levels to tidal predictions for the sites.

No tide gauges are installed near the study sites; hence, to calculate the annual lowest tides, we extracted tidal predictions from the Oregon State University tidal inversion model for the Indian Ocean region (available at http://people.oregonstate.edu/~erofeevs/IO.html; Egbert and Erofeeva, 2002). Details are in Appendix D and Table A3. To place all surveyed microatoll elevations into the tidal reference frame, we identified the optimal vertical shift at each site that minimizes the misfit between surveyed water levels and tidal predictions; this shift was then applied to all surveyed elevation data for the site. The lowest predicted tidal elevation in 2012 was defined as the datum for each site. Following this vertical shift and a correction at three sites for a systematic temporal offset between tidal predictions and surveyed water levels, the average misfit between surveyed and predicted water levels at any site is reduced to 13 mm or less, with the 2σ standard error of the mean at each site reduced to ± 18 mm or less (Appendix D; Table A4; Fig. A1). We suggest this temporal offset may result from an incorrect phase lag in at least one harmonic constituent in the tidal model, or from the influence of unmodeled or incorrectly modelled shallow-water tidal constituents.

Table 5
Elevations of the highest level of growth (HLG) on living microatolls relative to the lowest tide in 2012.

Site/Sample ID	Latitude (°N)	Longitude (°E)	Elevation of HLG (cm)
PNTN-A			
A-L1	4.08731	108.29444	32.4
A-L2	4.08731	108.29444	32.3
A-L3	4.08797	108.29395	36.2
A-L4	4.08826	108.29379	40.2
A-L5	4.08659	108.29397	32.7
PNTN-A mean ± standard deviation (σ)			34.8 ± 3.4
PNTN-C			
C-L1	3.99578	108.35572	27.1
C-L2	3.99579	108.35564	24.6
C-L3	3.99624	108.35553	23.9
C-L4	3.99518	108.35710	8.4
C-L5	3.99490	108.35719	−8.0
PNTN-C mean ± standard deviation (σ)			15.2 ± 14.9
PNTN-D			
D-L1	3.98421	108.37928	11.4
Overall			
Combined site mean ± standard deviation (σ)			23.7 ± 14.4

3.2.2. *Indicative meaning of microatoll HLG from living microatolls*

We identified a total of eleven living coral microatolls at the Natuna sites: five at PNTN-A, five at PNTN-C, and one at PNTN-D. No living microatolls were found at PNTN-B. We surveyed multiple HLG points on each microatoll. As noted by Smithers and Woodroffe (2000), microatolls with incomplete or locally depressed living rims are common,

and this can be caused by partial burial, bioerosion or physical damage. We avoided parts of the coral where the living HLG was locally (over a distance of a few decimetres) not uniform and visibly lower than a more extensive, uniform and higher HLG elsewhere on the coral, as these are places where we inferred that the HLG was not controlled by low-water level. This technique should be valid, as we surveyed the concentric rings of all fossil microatolls with the same approach. The values in Table 5 represent the average of the surveyed HLG elevations on each microatoll.

We take the mean of surveyed living *Porites* microatoll HLG (Table 5), 23.7 cm above the lowest predicted tide in 2012, as the reference water level. We use the standard deviation of surveyed living microatoll HLG elevations across all the sites, ± 14.4 cm, as a conservative estimate of the indicative range and the vertical error for each proxy sea-level index point. The indicative meaning for *Porites* microatoll HLG at the Natuna sites is therefore defined with a reference water level of 23.7 cm above the lowest predicted tide in 2012 and an indicative range of ± 28.7 cm (2σ).

We argue that the indicative range determined from living *Porites* HLG is a conservative estimate because the range of HLG on living microatolls should mimic or exceed that for individual generations of fossil microatolls. For any generation of microatolls, the spread of HLG is likely a function of the morphology of the reef, tidal range, and wave dynamics (Meltzner and Woodroffe, 2015). The reef morphology itself should have remained relatively constant over the study period. However, with higher RSL in the mid-Holocene, ponding may have been less of a factor, leading to a smaller scatter in HLG. The tidal range is unlikely to have changed significantly over this period: modelling by Meltzner et al. (2017) for Belitung, also on the Sunda shelf, showed that if RSL was 2 m higher than present, the low tide (in comparison to mean tide) would have been less than 10 cm different than at present. Furthermore, we assume no changes over time in *Porites* coral growth behavior. Changes over time in wave dynamics are more difficult to assess.

Some potential sources of error, however, are not captured in the indicative range. These factors vary by site and may present a systematic vertical bias at each site. Compaction is one potential source of error, but abundant granite outcrops at sites PNTN-C and PNTN-D suggest the corals are underlain by bedrock at those sites, and significant compaction is unlikely. Other potential factors include vertical tectonic land movement and GIA. These factors will require further study to fully assess. A first-order analysis using a recently developed GIA model for Southeast Asia by Bradley et al. (2016) indicates the spatial differences in RSL predictions between our study sites are < 0.1 m over the past 6 kyr. It is likely that since the distance between the four sites is small (less than 22 km between the farthest sites), any effects of tectonics and GIA would be similar at all sites, and their effects would lead to a similar systematic bias across all sites.

RSL at the time of growth of a particular microatoll ring is calculated as:

$$\text{RSL} = \text{HLG}–\text{reference water level} \quad (5)$$

The error in RSL is simply the uncertainties in modern and fossil HLG added in quadrature:

$$\sigma_{RSL} = \sqrt{{\sigma_{HLG}}^2 + {\sigma_{RWL}}^2} \quad (6)$$

where σ_{RSL}, σ_{HLG}, and σ_{RWL} are the errors in RSL, HLG (or HLS), and reference water level.

We note that for assessing RSL variability and RSL rates between 6400 and 1400 yr BP, the value of HLG (Eq. 4) and its uncertainty (the indicative range) should be used, as that uncertainty reflects the true uncertainty on one sea-level index point relative to another. However, for constraining GIA, where the absolute elevation of former RSL is critical and models assume zero uncertainty in present RSL, it is important to use RSL (Eq. 5) and its associated uncertainty (Eq. 6), as this incorporates the additional uncertainty in present RSL.

3.3. Porites microatoll growth rate analysis

An advantage of coral microatolls over traditional fixed biological indicators is that their morphologies record RSL histories over a finite period of time, not simply at an instant. These provide more complete records of RSL at a site, and also allow for estimates of rates of RSL change. However, unless an entire cross section of a microatoll is extracted, one must estimate a coral growth rate and extrapolate from individual dated samples.

In order to estimate a growth rate for all the Natuna Island *Porites* corals, we focus on one particularly large coral, microatoll PNTN-A-F4, for which we dated samples from two cores (Fig. 3; Supplementary Fig. S4). Samples PNTN-A-F4A and PNTN-A-F4B are from the second and ninth concentric rings of microatoll PNTN-A-F4, respectively, counting clearly identifiable rings inward from the outside. A rough estimate of the horizontal growth rate in PNTN-A-F4 is made by taking the radial distance between ring 2 (PNTN-A-F4A) and ring 9 (PNTN-A-F4B), 116.2 ± 2.6 cm (2σ), and dividing that by the difference in ^{230}Th ages between the two samples, 161 ± 12 yr (2σ), to give a horizontal growth rate of 0.721 ± 0.056 cm/yr (2σ). While this rate is within the range of commonly observed growth rates for *Porites* coral microatolls (0.5–2.5 cm/yr; Meltzner and Woodroffe, 2015), we note that this calculation assumes growth was in the horizontal direction and uniform along the growth direction. If this uniform growth direction deviated from perfectly horizontal (radially outward), the true growth rate would have been lower. Nevertheless, if these microatoll growth rates were sustained throughout the study period, it is appropriate to use the horizontal growth rate to extrapolate from the dated samples to estimate the age of successive concentric rings.

We also compare the 161 ± 12 year difference between the PNTN-A-F4A and PNTN-A-F4B samples with the 18.6-year periodicity of large die-downs that would be anticipated to result from the nodal tidal cycle at Natuna. There are a minimum of 7 concentric rings between PNTN-A-F4A and PNTN-A-F4B, which would correspond to one die-down on average every 23.0 ± 1.7 years (2σ). The calculated interval between die-downs would be smaller if there are additional die-downs that we failed to recognize from the surface morphology of the microatoll. This would be consistent with the hypothesis that microatoll morphology in Natuna Island is dominantly controlled by this 18.6-year tidal cycle.

3.4. Sea-level index points

We reconstruct sea-level index points by matching a ^{230}Th date, taken from a core drilled into a fossil microatoll, with the surveyed elevation of a point on the upper surface of the microatoll at the top of the core. The upper surface of the microatoll represents the HLG of the coral in a given year. This is a minimum limiting data point on RSL, but because of the microatoll's concentric annuli, any point on the upper surface is necessarily close to RSL, and with sufficiently large errors we can treat such data as sea-level index points.

Samples for ^{230}Th dating were all obtained at a depth below the upper surface (Table 6), in order to get a more pristine sample. Consequently, we must correct for the number of years it would have taken for the microatoll to grow from that depth to the upper surface.

To correct for the upward growth from the dated sample to the microatoll surface, we must consider the depth of the sample, the coral growth rate, and the local growth direction of the coral over that period. For a given sample depth and growth rate, if the coral had been growing vertically upward such that the growth bands were horizontal, then one would simply divide the depth by the growth rate to get the number of years it would have taken the coral to grow up to the top of the core. Alternatively, if the coral had been growing radially outward such that the growth bands were vertical, then there would be zero age difference between the dated sample and the top of the core directly above it. Because it is difficult to ascertain growth direction in some cores and because the growth direction is typically oblique

Table 6
Elevations of fossil microatolls relative to the lowest tide in 2012, and associated ^{230}Th dates.

Site/ Sample ID	Latitude (°N)	Longitude (°E)	Average elevation of highest concentric ring (cm)	Average elevation of lowest concentric ring (cm)	Elevation of top of core (cm)	Depth of ^{230}Th sample in core (cm)	^{230}Th age of sample[1] (yr BP) ± 2σ (weighted mean)	Age correction[1] for depth of sample ± 2σ (yr)	^{230}Th age of top of core[1] (yr BP) ± 2σ	Core location (estimated microatoll ring, counted inward from perimeter)
PNTN-A			**70.2**	**44.3**						
A-F1	4.08664	108.29447	70.2	64.1	69.8	7.0	1419 ± 8	−4.9 ± 4.9	1414 ± 10	2nd ring
A-F2	4.08738	108.29341	48.8	44.3	49.2	7.5	6183 ± 10	−5.2 ± 5.2	6178 ± 11	2nd ring
A-F3	4.08800	108.29380	53.4	50.9	51.0	17.0	5756 ± 19	−11.8 ± 11.8	5744 ± 22	4th ring
A-F4A	4.08805	108.29511	58.8	49.4	57.1	6.5	6178 ± 9	−4.5 ± 4.5	6173 ± 10	2nd ring
A-F4B					52.7	7.0	6339 ± 5	−4.9 ± 4.9	6334 ± 7	9th ring
PNTN-B			**60.9**	**38.7**						
B-F1	4.12012	108.24447	56.3	42.8	61.2	32.0	1932 ± 9	−22.2 ± 22.2	1910 ± 24	core from near centre of microatoll
B-F2	4.12103	108.24378	60.9	59.5	61.1	9.0	1776 ± 12	−6.2 ± 6.2	1770 ± 13	4th ring
B-F3	4.12232	108.24291	46.9	38.7	47.7	13.5	1714 ± 9	−9.4 ± 9.4	1705 ± 13	5th ring
PNTN-C			**78.3**	**66.1**						
C-F1	3.99685	108.35495	78.3	72.8	77.2	29.0	2953 ± 13	−20.1 ± 20.1	2933 ± 24	4th ring
C-F2	3.99588	108.35608	68.3	66.1	68.0	30.5	2277 ± 13	−21.2 ± 21.2	2256 ± 25	3rd ring
PNTN-D			**91.2**	**72.5**						
D-F1	3.98352	108.37812	72.5	72.5	72.9	19.0	3367 ± 16	−13.2 ± 13.2	3354 ± 21	2nd ring
D-F2	3.98504	108.37769	91.2	88.8	90.0	8.5	4696 ± 9	−5.9 ± 5.9	4691 ± 11	2nd ring

[1] The sample age was corrected to account for the depth of the sample in the core, assuming a coral growth rate of 0.721 cm/yr, and allowing for that growth to have been horizontal (radially outward), vertical (upward), or any angle in between (see Section 3.4).

(intermediate between horizontal and vertical), we calculate the number of years required for this growth assuming perfectly vertical growth and then halve this number. The result is our best estimate of the actual time required to grow from the sample depth to the upper surface. We set the 2σ uncertainty in this estimate as the range from the case of perfectly horizontal growth to that of perfectly vertical growth, i.e., ± 100% of the result itself. We assumed a *Porites* growth rate of 0.721 cm/yr, and the age corrections are listed in Table 6.

4. Results

4.1. Estimating ΔR

ΔR values estimated with paired ^{14}C (Table 1) and ^{230}Th (Table 2) dates from individual corals are shown on Table 4 and plotted on Fig. 4 as a function of time, typically ranging between about −40 and +40 yr (Marine13) or between about −210 and −100 yr (Marine20) except for an outlier in both cases (PNTN-A-F2). Though the ΔR estimate for PNTN-A-F2 is anomalously high, both ^{14}C and ^{230}Th measurements on that sample are consistent and reproducible, and we have no a priori reason to exclude this ΔR estimate as an outlier. We therefore include this value in our results to account for the inherent variability in ΔR as recommended by Russell et al. (2011).

Studies have shown that ^{230}Th dates from samples which have remained in closed systems for U and Th isotopes and are hence not diagenetically altered can be considered as absolute calendar ages (Bard et al., 1998). To identify any potential diagenetic alteration, we compared the sample's $\delta^{234}U_{initial}$ with the modern seawater δ^{234}U (Reimer et al., 2013b). The $\delta^{234}U_{initial}$ (corrected) of all our samples lie within 145 ± 7‰ and therefore suggest that diagenetic alteration, if any, is negligible (Table 2) (Cheng et al., 2013). This gives us confidence in using ^{230}Th dating as the independent chronometer for calibrating ^{14}C.

The IntCal criteria (Reimer et al., 2013b) for data used in radiocarbon calibration require that coral samples be acid-leached, and show < 1% residual calcite content to ensure low levels of secondary contamination to data. Though we did not perform x-ray diffraction to verify the calcite content of our coral samples, the reproducibility of our duplicate ^{14}C dating results (Table 3) affirms the reliability of our sample material. For U–Th dating, our samples have $\delta^{234}U_{initial}$ values within the modern range of 145 ± 7‰, which indicates the lack of significant diagenesis (Cheng et al., 2013). We conclude that our data fulfil the criteria stipulated by Reimer et al. (2013b) for use in estimating ΔR.

The resulting overall ΔR estimates for Natuna, 15 ± 63 yr (Marine13) or − 143 ± 176 yr (Marine20), are superimposed on Fig. 4. These estimates and their 1σ-uncertainties are reasonable, as the results lie within the scatter from uncertainties in their respective individual measurements (Southon et al., 2002).

4.2. Living microatoll HLG in Natuna

From the spread of living microatoll elevation in Natuna Island (Table 5), two observations can be made: (1) all living HLG from PNTN-A are at a higher elevation than their counterparts from other sites, and (2) there is considerable scatter in living HLG at PNTN-C. At least two hypotheses may explain the differences between the sites. Ponding, which allows for individual corals to grow above expected HLS, is a possible explanation for the consistently higher elevation of HLG at PNTN-A, as well as the scatter at PNTN-C. On wider reefs, the effect of ponding can raise the water level at low tides by more than 10 cm from the level of the ocean unaffected by ponding (Smithers and Woodroffe, 2000). Alternatively, some of the apparent variation in living HLG from one site to another may arise from our water-level measurements and the calculation of low tide at each site (Appendix D). Some of this scatter may result from unmodeled non-tidal sea level anomalies (Meltzner et al., 2010) or from water-level measurement error; either way, the apparent variation in HLG may exceed the true indicative range. Possibly insufficient water-level measurements, and a lack of sufficiently high-resolution imagery or bathymetric surveys of the reef that would allow for identification of potentially ponded areas, mean that neither hypothesis can be refuted.

The indicative range at Natuna spans the mean HLG elevations on all individual surveyed living *Porites* microatolls (Table 5), resulting in an indicative meaning of 23.7 ± 28.7 cm (2σ) above the lowest predicted tide in 2012. This range represents a wider distribution than in Belitung (± 18 cm, 2σ) (Meltzner et al., 2017), or off the west coast of Sumatra (± 8 cm, 2σ) (Meltzner et al., 2010). However, it is indistinguishable from the common HLG variation per site documented in Cocos (Keeling) Islands, Australia, where Smithers and Woodroffe (2000) calculated that variability in HLG for living open-ocean *Porites*

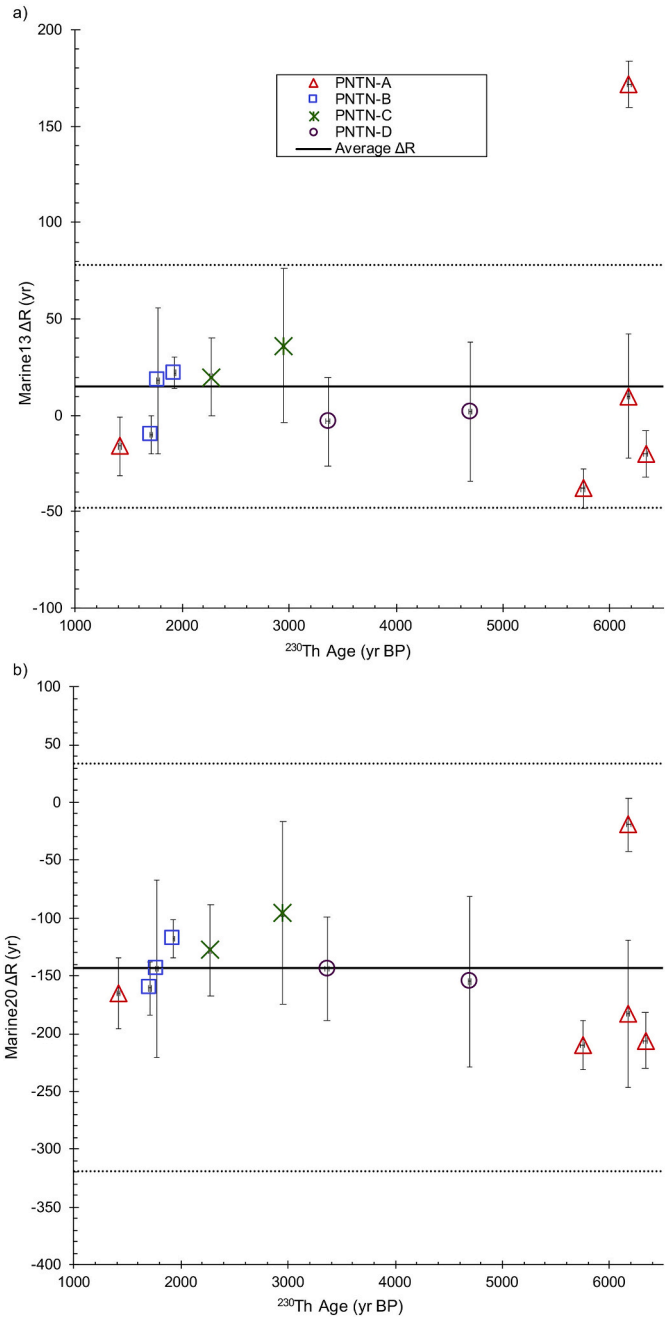

Fig. 4. ΔR over time obtained from paired ^{14}C and ^{230}Th ages of *Porites* coral samples from Natuna Island using a) Marine13, and b) Marine20 marine radiocarbon age calibration curves on *deltar*. Horizontal errors represent experimental uncertainty of ^{230}Th ages to 2σ; vertical errors (ΔR) are 1σ. Solid and dashed horizontal lines denote the weighted average of ΔR from all samples, plus or minus one weighted standard deviation.

microatolls was more than 10 cm per site at 9 of 19 sites, and more than 20 cm per site at 3 of 19 sites.

4.3. Mid-to-late Holocene RSL curve for Natuna Island

We plot the fossil microatoll elevations surveyed in Natuna Island in Fig. 5, based on microatoll proxy data in Tables 5 and 6. To avoid biasing our reconstructions of past RSL by measuring relative to HLS of ponded living corals, we plot the elevations of all fossil microatolls relative to the lowest tide in 2012 as described earlier. To visualize the indicative meaning of the fossil microatoll elevations, we plot the living microatoll elevations alongside the fossil microatoll elevations.

The fossil microatoll surfaces surveyed at our Natuna sites all lie between 0.39 ± 0.29 and 0.91 ± 0.29 m (2σ) above the lowest tide in 2012, despite their temporal spread (Table 6). We overlay the elevations and estimated relative ages of the successive concentric rings assuming a constant radial growth rate of 0.721 cm/yr on the plot of elevations and radiometrically-determined ages in Fig. 5.

If we subtract the reference water level, 0.24 ± 0.29 m (2σ), from these elevations, the result suggests that RSL was between 0.15 ± 0.41 and 0.68 ± 0.41 m above present (2σ) from 6400 to 1400 yr BP (Eqs. 5–6; Fig. 6).

Starting with the dated cores and the elevation of the microatoll surface at the top of each core, we "extended" the record from each microatoll in Figs. 5 and 6 using surveyed elevations of concentric microatoll annuli and an estimate of the age of each annulus based upon our estimated microatoll growth rate. These "extended" records are mostly consistent with one another. However, two "extended" data sets appear to contradict each other: contemporaneous microatolls at ~1600 yr BP suggest a falling RSL ~ 0.15 m higher than present at site PNTN-B, and a rising RSL ~ 0.40 m higher than present at site PNTN-A. This apparent contradiction is rectified if the growth rate of those corals was substantially faster than 0.721 cm/yr.

5. Discussion

5.1. A new ΔR estimate

We estimate ΔR for Natuna Island to be 15 ± 63 yr (1σ) (Marine13) or − 143 ± 176 yr (1σ) (Marine20) since at least the mid-Holocene. These estimates overlap the weighted averages of ΔR = −16 ± 39 yr (Marine13) or ΔR = −155 ± 38 yr (Marine20) calculated from the five *Porites* samples from the nearest regions listed in the ^{14}CHRONO Marine Reservoir Database (http://calib.org/marine13/ and http://calib.org/marine/ for Marine13 and Marine20, respectively). This lends confidence to the results. The five nearest samples were obtained from Con Dao Island, Vietnam, 550 km from Natuna (Dang et al., 2004); Hon Tre Island, Vietnam, 910 km from Natuna (Bolton et al., 2016); and Xisha (Paracel) Islands, Hainan, 1460 km from Natuna (Southon et al., 2002).

Any process that interferes with ^{14}C distribution can cause ΔR fluctuations. It is well established that ΔR is strongly spatially dependent, but whether ΔR can be considered stable over time at any location has been debated in the literature. Stuiver et al. (1986) defined ΔR and argued that ΔR should be roughly time-independent due to approximately parallel atmospheric forcing of the regional and global ocean. However, radiocarbon research on paleo-oceanic circulation suggests great variations in ΔR can occur during periods of extreme climate (Alves et al., 2018). In studies of the Younger Dryas, which was a cold-period at the end of the last glacial period between 12.9 and 11.7 kyr (Broecker et al., 2010), the variable effects of factors like change in advection of surface waters, monsoon upwellings and the ocean thermocline can contribute to variable surface ΔR fluctuations in the time period (e.g. Bard et al., 1994; Staubwasser et al., 2002). Indeed, research on the time dependency of ΔR in the South Pacific Gyre over the past 3000 years (Petchey et al., 2009; Petchey and Clark, 2011) indicates ΔR there is stable over time. Recent papers have challenged this assumption, however, arguing that variations in climate can result in a time-dependent ΔR (Yu et al., 2010), with Hughen et al. (2004) countering that changes in oceanic circulation patterns and deep-water upwelling may cause a temporal variation in ΔR. In a study of Holocene ^{14}C reservoir age variability based on corals from multiple sites in the South China Sea (all north of Natuna Island), Yu et al. (2010) suggest that fluctuations in ΔR could result from changing ENSO intensity and frequency, as well as variations in the East Asian monsoon, which affect upwelling in the Pacific Ocean and South China Sea, respectively. They argue that either a weakened ENSO or a strengthened East Asian

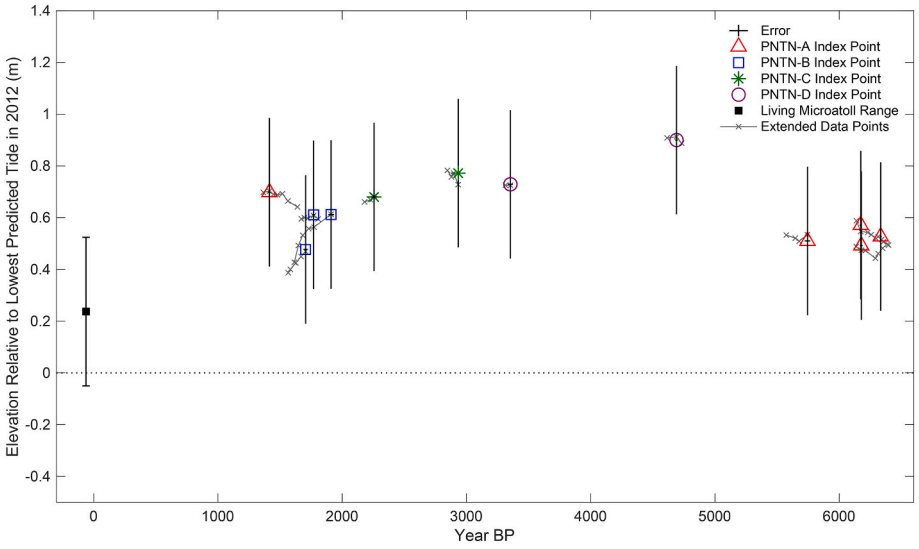

Fig. 5. Coral microatoll elevations at four sites on Natuna Island. Ages are based on ^{230}Th analyses. All elevations are taken relative to the lowest predicted tide in 2012. The average elevation of HLG on living microatolls at all four sites in 2012 is plotted with a 2σ vertical error. For fossil microatoll data, 2σ vertical (± 0.287 m) and 2σ ^{230}Th errors are plotted (^{230}Th error bars are obscured by the sea-level index point symbols). Different symbols correspond to data from different sites. Overlaid on the sea-level index points are lines signifying the growth history of each sampled microatoll, with surveyed elevations and estimated ages of successive concentric rings. This extension of the time series uses approximate coral growth rates estimated from two ^{230}Th-dated samples on microatoll PNTN-A-F4.

summer monsoon could lead to more positive ΔR values in the South China Sea, and observe recorded peaks in ΔR from 7500 to 5600 and from 3500 to 2500 cal yr BP in their dataset that correspond to reported weaker ENSO and stronger monsoon events in the South China Sea.

Our own calculations provide no evidence for temporal variability in ΔR. There is a single outlier, but ^{230}Th analyses suggest that the outlier (sample PNTN-A-F2, 6180 ± 5 yr BP (1σ), Marine13 ΔR = 172 ± 12 yr, Marine20 ΔR = −19 ± 23 yr) was of a similar age as another sample collected 200 m away at the same site (sample PNTN-A-F4A, 6175 ± 5 yr BP (1σ), Marine13 ΔR = 10 ± 32 yr, Marine20 ΔR = −183 ± 64 yr) (Table 4). For both samples, the ^{14}C and ^{230}Th measurements were independently reproducible (Table 3), suggesting that both ΔR determinations are robust. Therefore, we argue that the outlier reflects inherent variability in ΔR that is not readily explained as a function of time, and we include this value in our overall weighted-mean estimate for ΔR.

5.2. Natuna RSL

From 6400 to 1400 yr BP, Natuna RSL appears to have been between 0.2 and 0.7 ± 0.4 m (2σ) higher than present (Fig. 6). At every site, the surveyed elevation of the lowest sampled fossil microatoll was higher than the highest living microatoll HLG. Accounting for the indicative range, at 2σ vertical uncertainty, the upper surface elevations of most fossil microatolls overlap with HLG on only the highest living microatolls. An exception is PNTN-D-F2, whose entire indicative range is at a higher elevation than living microatolls surveyed across all sites.

The small vertical spread of RSL between 6400 and 1400 yr BP indicates prolonged RSL stability at Natuna for around 5000 years, before a fall to current RSL only after ~1400 yr BP. However, gaps exist in this record, most prominently between 5750 and 3360 yr BP, which is represented by a single microatoll. Efforts to find additional generations of fossil coral microatolls at Natuna Island are warranted. Any further interpretation of RSL changes between 6400 and 1400 yr BP is hampered by the large vertical errors.

5.2.1. A comparison to GIA models

Fig. 7 shows our proxy RSL data alongside GIA modelled RSL for Natuna Island using two published global ice sheet reconstructions: ICE6G (Argus et al., 2014; Peltier et al., 2015) and Bradley (Bradley et al., 2016). Bradley et al. (2016) developed an ice-sheet reconstruction constrained by RSL index points from China and the Malay-Thai Peninsula. It is characterised by a slowdown in LGM melt rates at ~7000 yr BP when the Laurentide ice sheet is inferred to have nearly completed melting, and continued eustatic sea level rise until ~1000 yr BP due to Antarctic ice melt. In contrast, in ICE6G there is rapid melting

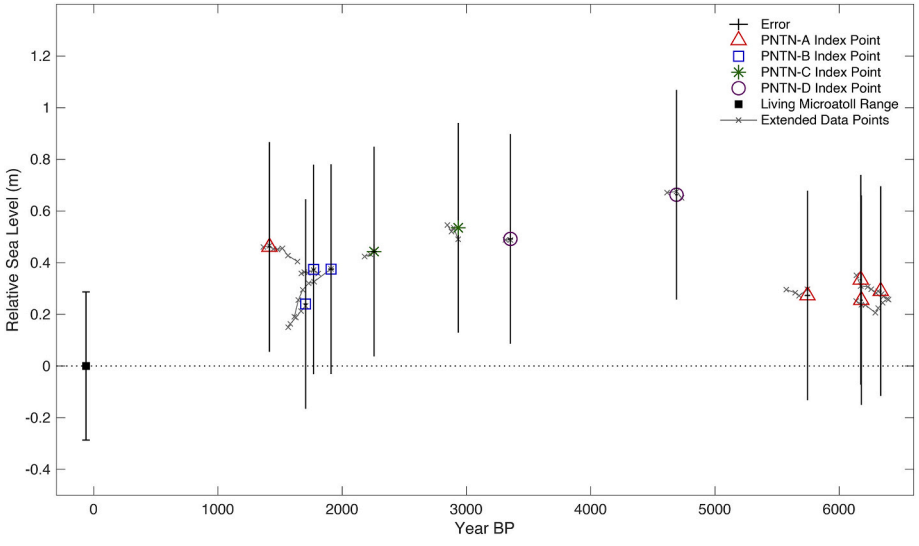

Fig. 6. Mid-to-late Holocene RSL at Natuna Island, based on coral microatolls. Present RSL is defined as the average living microatoll HLG across all sites, at 0.237 ± 0.287 m (2σ) above the lowest predicted tide in 2012 (Fig. 5). Past RSL is calculated as the difference between fossil microatoll HLG and living equivalents. Present-day RSL is set to zero here, but its associated uncertainty (arising from the spread of living microatoll HLG) propagates into the error for past RSL; this results in larger vertical errors (± 0.406 m (2σ)) here than in Fig. 5. 2σ ^{230}Th error bars are obscured by the sea-level index point symbols. Different symbols correspond to data from different sites.

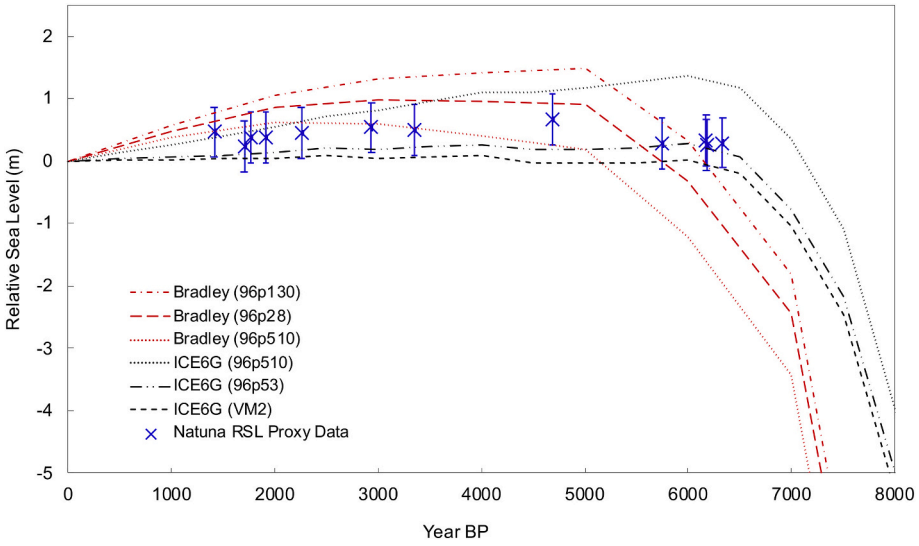

Fig. 7. GIA modelled RSL predictions for Natuna Island using two published global ice sheet reconstructions: ICE6G (Argus et al., 2014; Peltier et al., 2015) and Bradley (Bradley et al., 2016). Predictions from three rheological models each for Bradley and ICE6G are selected to encompass a range of earth and ice model combinations that predict RSL bounding our proxy data (blue points). See Appendix E, Table A5 for details on the rheological models. Proxy RSL data and uncertainties are from Fig. 6. 2σ ^{230}Th error bars for the RSL proxy data are small and therefore obscured by the data symbols. (For interpretation of the references to colour in this figure legend, the reader is referred to the web version of this article.)

between 12,000 and 5000 yr BP, with the major end of melting in Laurentide and Antarctica at ~8000 yr BP and ~6000 yr BP respectively. It is these differences in the timing of slowdown of melting of the major ice sheets which control the variation in timing of the RSL predictions described below. We chose to look at RSL predictions for each ice-sheet reconstruction combined with a selection of rheological models that best capture the new sea-level index point data and which comply with the statistical analysis of Bradley et al. (2016). That said, the effect of changing the rheological model broadly serves to shift the magnitude of RSL predictions, but these changes have less effect on rates of RSL rise prior to the highstand. A table of Earth model parameters from Bradley et al. (2016) can be found in Appendix E (Table A5), with details on VM2 given in Peltier (1996, 2004).

A comparison of the reconstructed RSL history and the aforementioned GIA model predictions reveals both a different preferred rheological model and style of predicted sea level that may roughly fit our reconstructed RSL history in Natuna Island (Fig. 7). The non-uniqueness of the choice of rheological models is perhaps to be expected as these are typically developed with the adopted ice-sheet reconstruction (e.g., VM2/VM5 for ICE6G). The Bradley reconstruction predicts a rise in RSL after 6000 yr BP, with a prolonged mid-Holocene highstand from 5000 to 2000 yr BP and subsequent fall towards present day. With the optimum rheological model from Bradley et al. (2016), 96p28, the reconstruction captures both the height of highstand (~1 m) and the fall towards present day, but it is unable to capture the elevated sea level at ~6400 yr BP.

Conversely, the ICE6G reconstruction predicts both an earlier rise towards present-day sea levels and an earlier highstand. ICE6G with rheological model 96p510, which has an upper-mantle viscosity of 0.5×10^{21} Pa·s and a lower-mantle viscosity of 10×10^{21} Pa·s, produces a significant highstand around 6000 yr BP. Combining ICE6G with a rheological model with a weaker lower-mantle viscosity (3×10^{21} Pa·s; 96p53) removes the pronounced highstand to produce a near-stable RSL at ~ +0.2 m from 6500 yr BP, capturing the lower limits of our sea-level index points. Although the development of new, optimal rheological models for the Natuna region is beyond the scope of this paper, it is apparent from Fig. 7 that an Earth model with a lower-mantle viscosity somewhere between 3×10^{21} and 10×10^{21} Pa·s, combined with ICE6G, could fit through the middle of many of the Natuna sea-level index points.

5.2.2. Timing of the mid-Holocene RSL highstand and complications elsewhere

Most published RSL reconstructions for Southeast Asia are based upon sea-level index points with meter-scale vertical and large temporal uncertainties (e.g. Geyh et al., 1979; Horton et al., 2005; Bird et al., 2010; Khan et al., 2015; Bradley et al., 2016), which permit a wide range of RSL histories at each site. Another study using high-precision coral microatolls from sites only ~300 km to the southeast in Sarawak, Malaysia, supports the contention from the Natuna reconstruction that RSL reached present levels and that RSL rise slowed earlier than predicted by the Bradley models. Majewski et al. (2018) showed that RSL was generally stable along the coast of Sarawak for at least a 300-yr period between 7400 and 7000 yr BP, contrary to the Bradley models' prediction of rapid (7–8 mm/yr) RSL rise over that period.

Additional support for RSL reaching present levels earlier comes from microatoll studies on Belitung Island, 750 km to the south, and the southern coast of China, 1800 km to the north. On Belitung, Meltzner et al. (2017) showed that RSL was 1.9 m above present by 6800 yr BP, and along the southern coast of China, Yu et al. (2009) showed that RSL was 1.9 m above present by 7000 yr BP. Although both RSL histories are complicated by ~0.6-m amplitude multidecadal RSL fluctuations between 7000 and 6500 yr BP, RSL was stable or falling on timescales of 300 yr or more over that interval. These observations generally contradict existing GIA models, which predict lower RSL at those sites at 7000–6800 yr BP, and RSL rise between 7000 and 6000 yr BP.

We further investigate if evidence of ~0.6-m amplitude mid-Holocene RSL fluctuations, as recorded on Belitung Island (Meltzner et al., 2017) and along the southern coast of China (Yu et al., 2009) between 7000 and 6500 yr BP, can be observed subsequently in Natuna Island. Meltzner et al. (2017) argued these fluctuations are likely basin-wide and may have resulted from regional climate variability like the El Niño-Southern Oscillation, the Pacific Decadal Oscillation or the Asian–Australian monsoon. If this were the case, we may expect similar fluctuations at Natuna Island. The lack of evidence from Natuna of similar RSL fluctuations between 6400 and 1400 yr BP suggests the fluctuations may have been limited to the period prior to 6400 yr BP, though the temporal discontinuities and larger vertical uncertainties in the Natuna proxy record leave open the possibility for small-scale fluctuations in RSL there. Notably, since our Natuna reconstruction starts after 6500 cal yr BP we cannot comment directly on the regional extent of the fluctuations recorded at Belitung and in southern China.

5.2.3. Mid-Holocene RSL elevations across the region

The mid-to-late Holocene RSL at Natuna was in general lower than Holocene RSL reported elsewhere on the Sunda Shelf, e.g. +1.5 m ~ 7000 cal yr BP along the northern coast of Central Java (Azmy et al., 2010); +1.9 m ~ 6800 cal yr BP on northwestern Belitung

Island (Meltzner et al., 2017); ~ + 2.5 m after 6500 cal yr BP in Singapore (Bird et al., 2010); and + 1.7 m (or up to + 2.4 m if a correction is needed for tectonic subsidence postdating the corals' growth) ~6100 yr BP in western Sarawak (Majewski et al., 2018). Past records that constrain the Holocene highstand on the Sunda Shelf suggest a maximum highstand of up to 5 m between 7000 and 4000 cal yr BP (Geyh et al., 1979; Kamaludin, 2003; Horton et al., 2005; Bird et al., 2010; Stattegger et al., 2013; Parham et al., 2014). This spatial variability in the elevation of the highstand can be attributed to isostatic effects (Horton et al., 2005).

Just beyond the Sunda Shelf, in the Spermonde Archipelago off southwestern Sulawesi, Mann et al. (2016) argue that RSL was 0.4 m above present ~5500 cal yr BP, based on elevations of corals. This inferred elevation of RSL is strikingly similar to the elevations we report at Natuna; however, we argue that this similarity is likely a mere coincidence, for several reasons: Firstly, the GIA signal since 5500 yr BP is not spatially uniform across the Sunda Shelf. For example, the effect of continental levering should be greater near the coast of a large land mass such as Sulawesi than on a smaller, more isolated island such as Natuna. Secondly, in contrast to the microatolls used in our study (Supplementary Figs. S1–S11), the photographs provided by Mann et al. (2016; see their figure 2 f–g), suggest their fossil corals were nearly flat, with no preserved concentric rings (or ridges) on the upper surfaces. Flat corals can result from abrasion and suggest that the upper part of the coral has been planed off. Mann et al. (2016) estimate that 0.2 m of vertical erosion occurred on some of their corals, but this is likely a minimum bound; there is no reason to discount the possibility that erosion exceeded 0.2 m. Moreover, if the top of a non-microatoll fossil coral (a hemispherical coral that had grown below low-water level) was planed off by erosion on an abrasion platform, such a coral would be indistinguishable from those shown by Mann et al. (2016); if that were the case, RSL at the time of those corals' growth could have been meters higher than the remnant, eroded surfaces.

Bender et al. (2020) supplemented the results of Mann et al. (2016) with new RSL data from corals on nearby islands. The Bender et al. (2020) correction for vertical erosion of the tops of the corals is somewhat more nuanced than the correction applied by Mann et al. (2016), but they still apply the correction only to a subset of their corals. However, like Mann et al., Bender et al. show only two example microatolls from their study (their figure 2), and both their “eroded” and “non-eroded” examples of fossil microatoll appear to be severely eroded; evidence for die-downs on the upper surfaces of those corals is not compelling in their photos (ironically, their “eroded” microatoll may preserve better evidence for concentric rings, despite the considerable amount of erosion that has taken place). We therefore surmise that the amounts of erosion assumed by Bender et al. (2020) may also significantly underestimate the actual erosion that has taken place.

Indeed, Mann et al. (2016) and Bender et al. (2020) compared the coral records from the Spermonde Archipelago with earlier findings of de Klerk (1982), who used various RSL proxies to infer that RSL there was ~2 m or more higher than present from ~6000 to ~1000 cal yr BP; earlier samples from Tjia et al. (1972) suggest RSL exceeded 5 m above present from ~5500 to ~4500 cal yr BP. Although Mann et al. (2016) suggest that the inconsistency between their results and the earlier work may have arisen from errors in the earlier work or from other problems with the earlier data, we suggest that the explanation could lie with the interpretations of Mann et al. (2016) and Bender et al. (2020). Specifically, if the elevations of Mann et al. (2016) and Bender et al. (2020) were adjusted more realistically for the likely amount of vertical erosion on their planed-off corals, their RSL reconstructions would be more consistent with the results of de Klerk (1982). Furthermore, recognizing that the process of continental levering is expected to drive strong spatial gradients in mid-Holocene RSL across the Maritime Continent of Southeast Asia (Horton et al., 2005; Meltzner et al., 2017), the higher RSL reconstructions of de Klerk (1982) should be expected for the Spermonde Archipelago, given its location so close to mainland Sulawesi.

5.2.4. Late Holocene to present-day RSL elevations in the region and beyond

RSL fall after the mid-Holocene highstand is not well resolved in past studies in the region (Geyh et al., 1979; Bird et al., 2010). Recent studies which constrain this fall indicate the behavior may vary regionally, for example, an oscillatory fall since 5000 cal yr BP in Merang, Malaysia, where RSL fell to − 0.6 m ~ 850 cal yr BP before rising back to present levels (Tam et al., 2018), compared to a linear 0.25 mm/yr fall from 5000 cal yr BP in southeastern Vietnam (Stattegger et al., 2013).

A more recent low-latitude RSL record comes from the Maldives in the central Indian Ocean. Using corals spanning the period since 1720 cal yr BP, Kench et al. (2020) argued for two low sea-level phases, during the periods 1720–1350 cal yr BP and 470–140 cal yr BP. Although only two or three of the Natuna corals overlap with the earlier Kench et al. lowstand (PNTN-A-F1, PNTN-B-F3, and possibly PNTN-B-F2; see Table 6) and none of our corals overlap with the more recent part of the Kench et al. record, our findings are generally inconsistent with those of Kench et al. In particular, while Kench et al. (2020) argue that RSL was 0.9 m lower than present during the earlier lowstand before rising rapidly to near-present levels, the PNTN-B microatolls argue that RSL at Natuna remained between 0.2 and 0.4 m above present from 1910 yr BP until ~1600 yr PB, and the PNTN-A-F1 microatoll suggests RSL rose to + 0.5 m by 1410 yr BP. Although the uncertainties on the Natuna elevations are not insignificant (Fig. 6), they do not permit a significant RSL drop like that proposed by Kench et al.

In light of these inconsistencies, we scrutinize the Kench et al. (2020) record. Like the corals examined by Mann et al. (2016), most or all of the Maldives corals appear to be severely planed off (Kench et al., 2020, their Supplementary fig. 3). A possible exception is coral 12 of Kench et al., which might have some concentric ring structure preserved, based on our interpretation of their supplementary fig. 3b. It is noteworthy that coral 12 was 0.4 m higher than other, more planar-topped coeval corals in their data set, and we suggest that this was because the other corals were all eroded farther downward. However, Kench et al. discarded coral 12 as an outlier (they speculated that coral 12 may have been ponded) and based their RSL reconstruction on the lower, planed-off corals. Kench et al. did not adjust their surveyed elevations to account for possible erosion. Based on our reinterpretation of the Kench et al. (2020) record, we argue that their coral 12 represents the best approximation of RSL in the Maldives at the time, although coral 12 has also sustained significant erosion and therefore also provides a minimum bound on RSL. In light of this, the earlier lowstand of Kench et al. (2020), if real, was likely no lower than 0.4 m below present (2018) levels.

The problems in the studies of Mann et al. (2016), Bender et al. (2020), and Kench et al. (2020) highlight the importance of finding corals with concentric rings on their upper surfaces, as seen in Supplementary Figs. S1–S11 of this study. A flat planar surface on a coral does not by itself indicate that a coral was ever a microatoll, as the flat surface could result from abrasion and planing off of the upper part of a non-microatoll coral. At best, even if the flat-topped coral was a microatoll, the now-planar surface implies the coral has sustained substantial downward erosion since it grew.

5.2.5. General observations

The RSL reconstruction from Natuna is consistent with nearby and regional reconstructions but adds critical new constraints on RSL history. Comparison with two GIA models show potential consistency between our observations and GIA model predictions for Natuna Island, particularly after changes in the rheological model which serve to shift the magnitude of the GIA predictions. Future work on revising ice sheet reconstructions and companion rheological models for GIA predictions which can be compatible with the increasingly dense Holocene RSL proxy data from the Sunda Shelf is outside the scope of this paper. To

this end, the Natuna reconstruction may be an important constraint to capture the associated GIA model complexities. We underscore the importance of rigorous assessment of existing RSL reconstructions based on microatoll data in future efforts to utilize these records.

6. Conclusions

We have developed a high-resolution RSL curve for Natuna Island spanning 6400 to 1400 yr BP using high-precision ^{230}Th dating, which constrains a five-thousand-year period of prolonged RSL stability between 0.2 and 0.7 ± 0.4 m (2σ) above present levels. Our results suggest a more recent fall in RSL in far-field Natuna Island to present-day elevations that began sometime after 1400 yr BP. Comparison of our results with GIA predictions reveal rough similarities but suggest modifications to published ice-history models may be necessary.

We also produced a new ΔR estimate for the radiocarbon marine reservoir correction for Natuna Island, from paired ^{14}C and ^{230}Th analyses of fossil coral samples. We estimate that ΔR = −143 ± 176 yr (Marine20) [ΔR = 15 ± 63 yr (Marine13)] from 6400 to 1400 yr BP, with no obvious time-dependency during that period.

Supplementary data to this article can be found online at https://doi.org/10.1016/j.margeo.2020.106342.

Acknowledgements

Primary funding for this work came from the National Research Foundation Singapore and the Singapore Ministry of Education under the Research Centres of Excellence initiative. This research was also supported by the National Research Foundation Singapore under its Singapore NRF Fellowship scheme (Awards NRF-RF2010-04 to A.D.S., NRF-NRF2011-08 to X.W., and NRF-NRFF11-2019-0008 to A.J.M.). B.P.H. was supported by the Singapore Ministry of Education Academic Research Fund (Awards MOE2018-T2-1-030 and MOE2019-T3-1-004). S.L.B. acknowledges support from the European Research Council (Award ERC-StG-678145-CoupledIceClim). We thank D. Prayudi and I. Suprihanto for field support, and two anonymous reviewers for helpful suggestions that significantly improved the quality of this manuscript. This paper results from joint-research activities between the Earth Observatory of Singapore–Nanyang Technological University and the Research Center for Geotechnology LIPI. This paper is a contribution to PALSEA2 (Paleo-Constraints on Sea-Level Rise 2) and to International Geoscience Programme (IGCP) Project 639, 'Sea Level Change from Minutes to Millennia'. This is Earth Observatory of Singapore contribution no. 211.

Declaration of Competing Interest

The authors declare that they have no known competing financial interests or personal relationships that could have appeared to influence the work reported in this paper.

Appendix A. Dating methods

A.1. ^{14}C dating method

Twenty-four ^{14}C ages were measured for the 12 coral cores (Table 1). Samples were sub sampled by crushing using a hammer and chisel and manually scraped to obtain clean pieces. Sample surfaces were etched with 0.5 M HCl for 2 min to leach surface contamination before being rinsed and dried in a vacuum oven. The cleaned and etched material was crushed into powder and a further sub sample was reacted with 85% orthophosphoric acid in a closed evacuated vessel. The evolved CO_2 was collected, quantified, and cryogenically purified. Sample CO_2 was reduced to graphite by reduction over an iron catalyst in the presence of hydrogen gas (Turnbull et al., 2015).

Graphite ^{14}C/^{13}C ratios were measured by accelerator mass spectrometry incorporating all three carbon isotopes (Zondervan et al., 2015). The ratios were standardised via Oxalic Acid I and results are corrected for ^{14}C blank and normalised to δ^{13}C of −25‰ (Zondervan et al., 2015; Stuiver and Polach, 1977). Typical measurement uncertainties are 0.2–0.3% and are determined from a combination of the counting statistical uncertainty for the individual sample and the long-term repeatability of standard materials. Since sufficient sample was available, we provide environmental δ^{13}C values measured separately with an IRMS (pre-graphitization; Table 3). All sample preparation and measurements were conducted in the Rafter Radiocarbon Laboratory, Institute of Geological and Nuclear Sciences in New Zealand.

A.2. ^{230}Th dating method

Seventeen ^{230}Th ages were measured for the 12 coral cores (Table 2). Samples were gently crushed into 1- to 3-mm^3 fragments. Then, we selected clean and pristine pieces under a microscope, and physically cleaned the samples with ultrapure water three times using an ultrasonic cleaning machine. Samples were then dried in an oven at ~50 °C.

For each sample, ~20 mg was used for U–Th chemistry. Replicates were prepared for five subsamples (A-F1, A-F2, A-F4A, A-F4B and D-F2). All the samples were dissolved in ultrapure nitric acid, and a ^{229}Th–^{233}U–^{236}U mixed spike was then added to the solution. Drops of $HClO_4$ were added to remove organic compounds. Each sample solution was refluxed at 175 °C for 2 h and dried. To re-dissolve the dried samples, 2 N ultrapure HCl solution was added. Then, co-precipitation was achieved by adding $FeCl_3$ and concentrated NH_4OH. The co-precipitates were re-dissolved and put through an anion-exchange resin in columns to separate and purify uranium and thorium. U and Th fractions were then dissolved in 1% HNO_3 (+0.1% HF) for instrumental analysis. The detailed chemical protocols largely follow those described by Edwards et al. (1987) and Shen et al. (2012).

U and Th isotopic compositions were determined on a Neptune Plus multi-collector inductively coupled plasma mass spectrometer (MC-ICP-MS) housed in the isotope geochemistry laboratory at the Earth Observatory of Singapore (EOS) and Asian School of the Environment (ASE), Nanyang Technological University, Singapore. The measurements were done using a recently improved SEM peak-jumping technique (Cheng et al., 2013; Chiang et al., 2019). Except for ^{238}U and ^{232}Th, all other U and Th isotopes were measured in a peak-jumping mode on a secondary electron multiplier (SEM) equipped with a retarding potential quadruple (RPQ) lens for abundance sensitivity improvement. Half-lives of ^{234}U and ^{230}Th were adopted from Cheng et al. (2013), together with the half-life of ^{238}U from Jaffey et al. (1971). The corrected ^{230}Th ages are calculated assuming an initial ^{230}Th/^{232}Th atomic ratio of $(4.4 \pm 2.2) \times 10^{-6}$, a value for material at secular equilibrium, and a bulk Earth ^{232}Th/^{238}U value of 3.8. As the ^{230}Th/^{232}Th atomic ratios are high in all the samples, this initial correction is mostly negligible. The uncertainties for the U–Th dates are reported at 2σ level unless stated otherwise.

Appendix B. Calculation of standard error for duplicate dating results

In the main text we adopt the scale-corrected standard error of the weighted mean ($\hat{\sigma}_{\bar{x}}$) to calculate duplicate ^{14}C and ^{230}Th ages. This includes the reduced-χ^2 term, which corrects the standard error of the weighted mean to account for over- or under-dispersion among the duplicate ages. However, by convention the standard error of the weighted mean of duplicate ^{230}Th results is not calculated using the reduced-χ^2 term; instead what is commonly reported for ^{230}Th results is the uncorrected standard error of the weighted mean ($\sigma_{\bar{x}}$):

$$\sigma_{\bar{x}} = \sqrt{\frac{1}{\sum_{i=1}^{n} \sigma_i^{-2}}}$$

We compare the results from both methods of calculating the associated error in Table A1. The scale-corrected standard error of the weighted mean ($\hat{\sigma}_{\bar{x}}$) yields $\Delta R = 15 \pm 63$ yr, whereas the uncorrected standard error of the weighted mean ($\sigma_{\bar{x}}$) yields $\Delta R = 13 \pm 48$ yr (for both, ΔR was calculated for Marine13, with 1σ uncertainties). The difference in ΔR estimated from either error calculation method is not large, where removing the reduced-χ^2 term increases the uncertainty for each sample but results in an overall reduction of error in ΔR.

Appendix C. ΔR estimates from *deltar* and OxCal

In addition to using *deltar*, we also estimated ΔR using OxCal (Bronk Ramsey, 2009). To estimate ΔR for an individual sample, we used the Combine() functionality in OxCal to link the ^{14}C and offset ^{230}Th ages, in order to determine a probability distribution function for ΔR; to estimate a joint ΔR for all the samples from the Natuna sites, we put all of the combined dates for the respective samples in a Phase(), imposing a common ΔR for the phase. As a prior for ΔR, we adopted a uniform likelihood distribution between -400 and $+400$ years. The OxCal scripts are provided in the Supplementary Text. The posterior distributions for ΔR are centered nearly perfectly on the respective values estimated using *deltar* (Table A2). Furthermore, for both Marine13 and Marine20, the joint ΔR estimate for all the samples from Natuna, a single value of ΔR that best fits all the age data, is nearly identical to the overall estimate of ΔR, which is calculated according to Eqs. 1 and 3, and captures the variance in ΔR in the data set. The primary difference between the joint and overall estimates of ΔR is in the size of the error itself. If applying radiocarbon techniques to estimate the age of a new marine sample from the Natuna vicinity, the larger ΔR uncertainties should be adopted.

Appendix D. Methodology to reconstruct RSL from fossil microatolls

Ideally, reconstruction of a site's RSL history would involve the extraction of fossil microatoll slabs using the methodology of Meltzner and Woodroffe (2015). This technique involves digitally mosaicking and annotating microatoll slab x-rays, identifying coral die-downs and counting annual density bands between them, and determining the elevation of each annual band to reconstruct RSL as recorded by the microatoll. However, logistical constraints precluded the collection of slabs from Natuna Island. Instead, we utilize accurately surveyed points on the concentric rings on the surface of each microatoll, combined with geochronological analyses of samples extracted from cores into each microatoll, to produce sea-level index points illustrating the RSL history of Natuna Island. Some of the steps undertaken to produce sea-level index points from microatolls in Natuna Island are elaborated on below.

D.1. Surveying elevations

We used a total station to survey points along the crest of each concentric annulus on the surface of sampled fossil microatolls. Multiple points were surveyed on each concentric ring, to check for tilting and to account for local variation in the elevation of a microatoll. We also surveyed the water level at multiple times at each site, noting the exact time of each measurement, to allow us to put all surveyed elevations into a tidal reference frame. Where identified, we also surveyed the HLG on living coral microatolls, to establish the relationship between microatoll elevation and RSL and its vertical uncertainty (Meltzner and Woodroffe, 2015).

D.2. Fitting multiple site survey elevations to a common datum

In order to compare fossil coral elevations across all sites, we placed surveyed elevations relative to a common datum – the lowest predicted tidal elevation for calendar year 2012 at the site.

There are no available tide gauge data in close proximity to the study sites; hence, to calculate the lowest annual tide, we utilised tidal predictions from the Oregon State University regional tidal inversion model (Egbert and Erofeeva, 2002). Tide predictions for Natuna Island can be extracted from both the Indian Ocean region (IO) model (available at http://people.oregonstate.edu/~erofeevs/IO.html) and the China Seas region (CS) model (available at http://people.oregonstate.edu/~erofeevs/YS.html). We compared tidal predictions for calendar year 2012 from both models and summarise the results in Table A3. We found negligible differences between tidal predictions from either model at PNTN-A and PNTN-B. The consistency between models gives us confidence in the vertical accuracy of the tidal predictions. Since both models are similar, and the CS model provides no prediction for PNTN-C, we chose the IO model for subsequent calculations. However, the difference between the two models for PNTN-D is comparatively large (the average magnitude of the difference at this site is 18.6 mm) and suggests slightly larger uncertainties for the tidal predictions for sites PNTN-C and PNTN-D.

Using the extracted IO model tidal predictions, we calculated the optimum vertical shift in reference frame that would minimize the misfit between the surveyed water levels and contemporaneous tidal predictions. We shifted all surveyed elevations, including those of water levels and microatoll surfaces, by this amount, such that all elevations were now given with respect to the lowest predicted tidal elevation in 2012 at each site (Tables 5 and 6).

Despite implementing the vertical shift that minimized the misfit between surveyed and predicted water levels, a significant misfit remained (Fig. A1, upper panel; Table A4, column 3). We noticed that by uniformly shifting the tidal predictions along the temporal axis, the average misfit between

surveyed and predicted water levels could be reduced further. Optimum temporal offsets of +20, +15, and +21 min of tidal predictions at sites PNTN-A, -B, and -C, respectively, were found to drive the average misfit between surveyed and predicted water levels down to 13 mm or less (Fig. A1, lower panel; Table A4, column 4). The good fit between our data and the tidal predictions provides confidence in the tide model, in our measurements, and in the suitability of using the lowest predicted tidal level of 2012 as the common datum.

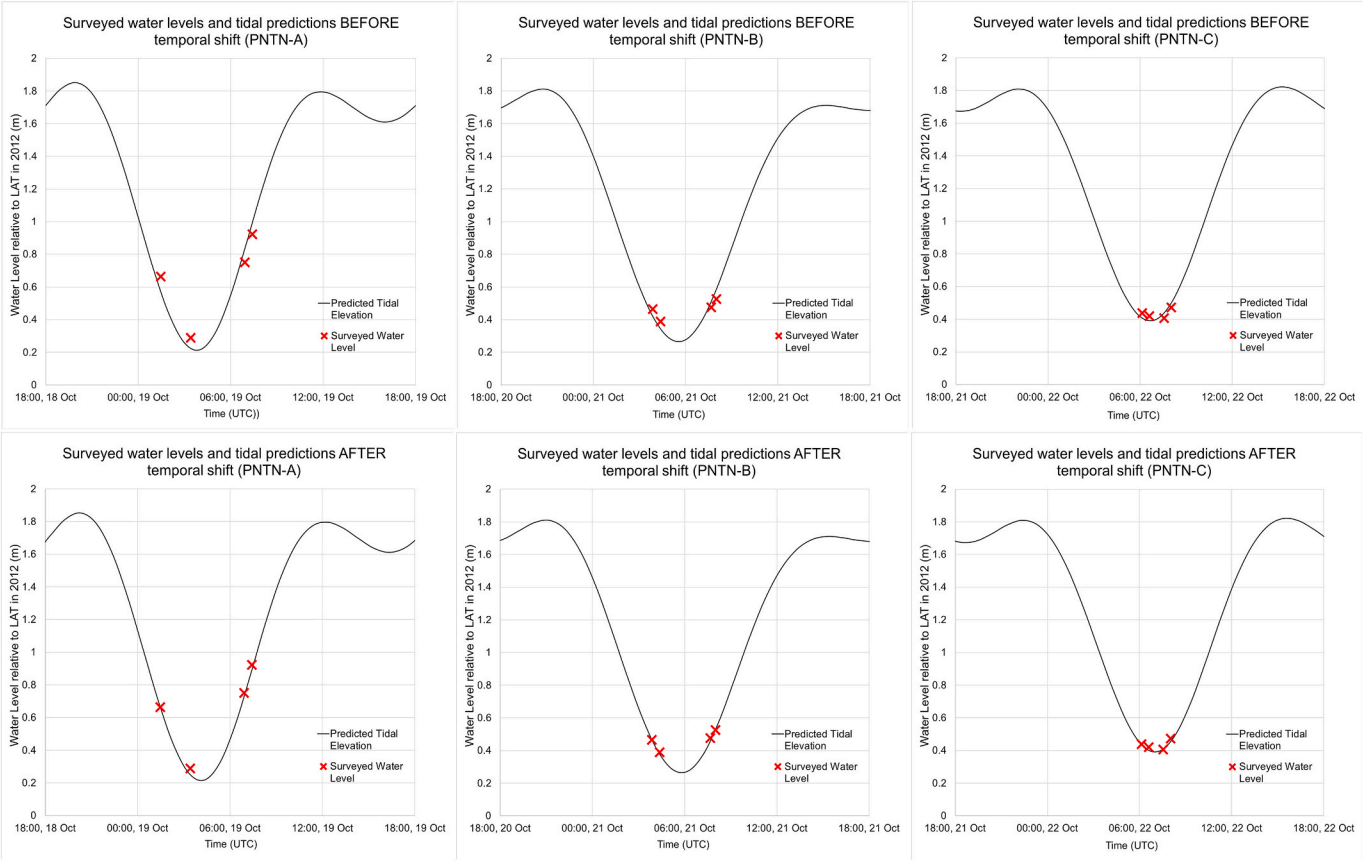

Fig. A1. Comparison of surveyed water levels with tidal predictions at the PNTN-A (left), PNTN-B (center), and PNTN-C (right) sites. The upper panel shows the fit at each site without any temporal shift in the modeled tides. The lower panel shows the improved fits after optimal temporal shifts in the modeled tides at each site. Details are in Appendix IV, Section A4.2, and in Table A4.

D.3. Challenges in reconstructing paleo-RSL

To interpret coral HLS as a function of RSL, one must make informed assumptions about the local influence of storms, terrestrial sedimentation, and other effects (Ryan et al., 2016). Fortunately, at 4°N, Natuna Island does not experience tropical cyclones or typhoons, so storms should not have a large influence at our sites. Environmental limitations can also affect the sensitivity of coral microatolls to RSL changes. Corals of the same species are not necessarily found at a uniform elevation. Instead, they vary according to local wave exposure, which is affected by the morphology of the coast. Change in RSL over millennia may have altered the wave dynamics at each location, but for this study we assume that any effects of changes in wave dynamics are captured by the indicative range of microatoll HLG. A more significant impact of reef morphology is the effect of ponding. Ponding is a phenomenon which arises when enclosed, elevated pools of water that do not drain at low tide are found on the reef, allowing microatolls which grow within these pools to survive at higher elevations than they could otherwise. We again assume that the effects of ponding are captured by the indicative range of microatoll HLG.

Erosion of the microatoll surface raises significant uncertainty, particularly in the case of fossil microatolls that have been exposed to the elements for thousands of years. Evidence of die-downs, and the highest level of growth a coral reaches at any year can often be eroded away. However, evidence from microatoll slabs at other sites (Meltzner et al., 2017) suggests that, where concentric rings are well preserved, vertical erosion is not more than ~5 cm; such appears to be the case for the majority of the sampled Natuna microatolls.

It must also be acknowledged that microatoll formation might also be caused by current, excessive sedimentation and nutrient uptake. However, in reef-flat settings, sea level is often the dominant driver of microatoll formation (Yu et al., 2009).

Appendix E. Rheological parameters used in GIA models for Natuna Island

Table A5 contains the Earth model parameters used with the Bradley et al. (2016) GIA models for Natuna Island.

Table A1
Comparison of ΔR (Marine13) estimates based on two methods[1] of calculating standard error of the weighted mean.

Site/ Sample	Corrected ^{230}Th Age (yr BP) ± 2σ[2]								Conventional ^{14}C Age (rcy BP) ± 1σ[2,3]					ΔR (yr) ± 1σ[4]			
ID	Individual dates		Weighted mean			WM offset by −3 ± 4 yr			Individual dates		Weighted mean			*deltar* result (Marine13)			
				$\hat{\sigma}_{\bar{x}}$ method	$\sigma_{\bar{x}}$ method		$\hat{\sigma}_{\bar{x}}$ method	$\sigma_{\bar{x}}$ method				$\hat{\sigma}_{\bar{x}}$ method	$\sigma_{\bar{x}}$ method	$\hat{\sigma}_{\bar{x}}$ method		$\sigma_{\bar{x}}$ method	
PNTN-A																	
A-F1	1427.5	± 22.8	1419.3	± 8.2	± 16.1	1416.3	± 9.1	± 16.6	1888	± 27	1873.0	± 14.5	± 18.7	−16	± 15	−13	± 20
	1411.1	± 22.8							1859	± 26							
A-F2	6172.7	± 23.7	6182.9	± 9.5	± 16.1	6179.9	± 10.3	± 16.6	5930	± 28	5922.3	± 8.0	± 20.1	172	± 12	176	± 24
	6191.7	± 22.0							5914	± 29							
A-F3	5756.3	± 18.9	5756.3	± 18.9	± 18.9	5753.3	± 19.4	± 19.4	5360	± 28	5363.9	± 4.0	± 20.1	−38	± 10	−36	± 22
									5368	± 29							
A-F4A	6189.7	± 30.9	6177.9	± 8.6	± 18.3	6174.9	± 9.5	± 18.7	5706	± 42	5750.7	± 30.9	± 23.9	10	± 32	10	± 28
	6171.6	± 22.6							5772	± 29							
A-F4B	6344.0	± 22.5	6338.7	± 5.3	± 15.9	6335.7	± 6.6	± 16.4	5902	± 28	5913.5	± 11.5	± 19.8	−20	± 12	−21	± 20
	6333.4	± 22.6							5925	± 28							
PNTN-B																	
B-F1	1932.0	± 9.3	1932.0	± 9.3	± 9.3	1929.0	± 10.1	± 10.1	2335	± 27	2341.7	± 6.5	± 18.7	22	± 8	22	± 19
									2348	± 26							
B-F2	1776.1	± 11.9	1776.1	± 11.9	± 11.9	1773.1	± 12.5	± 12.5	2153	± 25	2189.5	± 38.0	± 18.0	18	± 38	18	± 18
									2229	± 26							
B-F3	1714.3	± 9.2	1714.3	± 9.2	± 9.2	1711.3	± 10.0	± 10.0	2113	± 25	2122.1	± 9.5	± 18.0	−10	± 10	−10	± 18
									2132	± 26							
PNTN-C																	
C-F1	2953.1	± 12.9	2953.1	± 12.9	± 12.9	2950.1	± 13.5	± 13.5	3145	± 40	3202.7	± 39.0	± 22.4	36	± 40	36	± 23
									3229	± 27							
C-F2	2277.0	± 12.6	2277.0	± 12.6	± 12.6	2274.0	± 13.2	± 13.2	2598	± 25	2580.2	± 18.5	± 18.0	20	± 20	20	± 19
									2561	± 26							
PNTN-D																	
D-F1	3366.8	± 15.8	3366.8	± 15.8	± 15.8	3363.8	± 16.3	± 16.3	3451	± 40	3481.2	± 20.4	± 22.4	−3	± 23	−4	± 24
									3495	± 27							
D-F2	4705.0	± 25.5	4696.5	± 8.9	± 18.3	4693.5	± 9.7	± 18.8	4457	± 27	4492.2	± 36.5	± 19.4	2	± 36	2	± 20
	4687.3	± 26.4							4530	± 28							
Overall ΔR (1σ)														**15**	**± 63**	**13**	**± 48**

[1] $\hat{\sigma}_{\bar{x}}$ is the scale-corrected standard error of the weighted mean, as used in the main text and Tables 2–4. $\sigma_{\bar{x}}$ is the uncorrected standard error of the weighted mean. See Appendix B for details.
[2] BP is "before present" where the "present" is defined as the year 1950 CE.
[3] rcy is "radiocarbon years".
[4] ΔR estimates calculated using the *deltar* programme for Marine13 (from http://calib.org/deltar13/).

Table A2
Comparison of ΔR estimates based on *deltar* and OxCal.

Sample ID[1]	ΔR (yr) ± 1σ for Marine13				ΔR (yr) ± 1σ for Marine20			
	from *deltar*[1]		from OxCal[2]		from *deltar*[1]		from OxCal[2]	
PNTN-A-F1	−16	± 15	−15	± 27	−165	± 31	−164	± 44
PNTN-A-F2	172	± 12	173	± 31	−19	± 23	−18	± 54
PNTN-A-F3	−38	± 10	−39	± 28	−210	± 21	−212	± 51
PNTN-A-F4A	10	± 32	7	± 35	−183	± 64	−191	± 56
PNTN-A-F4B	−20	± 12	−20	± 28	−206	± 24	−206	± 51
PNTN-B-F1	22	± 8	23	± 26	−118	± 17	−118	± 45
PNTN-B-F2	18	± 38	20	± 27	−144	± 77	−142	± 44
PNTN-B-F3	−10	± 10	−10	± 26	−161	± 23	−160	± 44
PNTN-C-F1	36	± 40	31	± 31	−96	± 79	−107	± 47
PNTN-C-F2	20	± 20	22	± 27	−128	± 40	−125	± 46
PNTN-D-F1	−3	± 23	−6	± 31	−144	± 45	−149	± 48
PNTN-D-F2	2	± 36	4	± 27	−155	± 74	−153	± 48
Joint[3] ΔR for PNTN			15	± 9			−145	± 14
Overall[4] ΔR for PNTN	15	± 63	14	± 51	−143	± 176	−145	± 173

[1] Values as in Table 4.
[2] ΔR estimates from the OxCal program (Bronk Ramsey, 2009) are based on Bayesian methodologies. Details are in Appendix C and Supplementary Text.
[3] The joint ΔR is determined from the OxCal scripts in the Supplementary Text, and is a single value of ΔR that best fits all the age data from the PNTN sites.
[4] The overall ΔR is calculated according to Eqs. 1 and 3, and captures the variance in ΔR in the data set.

Table A3
Comparison of tide predictions from the IO and CS tidal inversion models.[1]

Site	Latitude (°N)	Longitude (°E)	Lowest predicted water level (2012)		Difference in tide predictions by IO and CS models	
			IO model (m)	CS model (m)	Average (m)[2]	Standard deviation (m)
PNTN-A	4.0876	108.2942	−1.2892	−1.3346	0.0049	0.0183
PNTN-B	4.1218	108.2436	−1.2453	−1.3242	0.0050	0.0332
PNTN-C	3.9958	108.3563	−1.3296	no prediction	–	–
PNTN-D	3.9846	108.3785	−1.3346	−1.3497	0.0186	0.0180

[1] IO is Indian Ocean. CS is China Seas. Both models are discussed in Appendix D.2.
[2] We define the *average difference in tide predictions* as the average over all time steps of the magnitude (the absolute value) of the difference between the two models' predictions of tidal elevation at a particular time step.

Table A4
Reduction of misfit following temporal shift of tidal predictions.

Site	Temporal shift (minutes)	Average of the absolute value of the misfit[1] between IO tidal prediction and surveyed water levels (m)		2σ standard error of the mean of the misfit[1] between IO tidal prediction and surveyed water levels (m)	
		Before temporal shift	After temporal shift	Before temporal shift	After temporal shift
PNTN-A	+20	0.079	0.013	0.092	0.018
PNTN-B	+15	0.045	0.008	0.053	0.010
PNTN-C	+21	0.031	0.010	0.035	0.013
PNTN-D	0	0.008	0.008	0.012	0.012

[1] For each surveyed water level, we calculated the misfit as the difference between the measured water level and the predicted tidal elevation corresponding to the time of the measurement. Columns 3 and 5 show the average misfit and the standard error of the mean of the misfit after applying the optimum vertical shift in reference frame to minimize this misfit, but without any temporal shift. Columns 4 and 6 show these values after also applying the optimum temporal shift. See Appendix D.2 for details.

Table A5
Rheological parameters used in GIA models for Natuna Island.[1,2]

Model	96p28	96p130	96p510	96p53
Lithosphere thickness (km)	96	96	96	96
Upper mantle viscosity (Pa·s)	2×10^{20}	1×10^{20}	5×10^{20}	5×10^{20}
Lower mantle viscosity (Pa·s)	8×10^{21}	3×10^{22}	1×10^{22}	3×10^{21}
χ^2 misfit to Malay-Thai Peninsula data set	15.61	22.05	25.47	16.88

[1] A selection of earth model parameters used in the χ^2 analysis of Bradley et al. (2016). The 95% confidence limit of χ^2 misfit is 25.2 for the original Malay–Thai Peninsula data.
[2] For details of the VM2 model, see corresponding literature by Peltier (1996, 2004).

References

Alves, E.Q., Macario, K., Ascough, P., Bronk Ramsey, C., 2018. The worldwide marine radiocarbon reservoir effect: definitions, mechanisms, and prospects. Rev. Geophys. 56, 278–305. https://doi.org/10.1002/2017RG000588.

Azmy, K., Edinger, E., Lundberg, J., Diegor, W., 2010. Sea level and paleotemperature records from a mid-Holocene reef on the North coast of Java. Indonesia. Int. J. Earth Sci. (Geol. Rundsch.) 99, 231–244. https://doi.org/10.1007/s00531-008-0383-3.

Argus, D.F., Peltier, W.R., Drummond, R., Moore, A.W., 2014. The Antarctica component of postglacial rebound model ICE-6G_C (VM5a) based on GPS positioning, exposure age dating of ice thicknesses, and relative sea level histories. Geophys. J. Int. 198, 537–563. https://doi.org/10.1093/gji/ggu140.

Baker, R.G.V., Haworth, R.J., 2000a. Smooth or oscillating late Holocene sea-level curve? Evidence from cross-regional statistical regressions of fixed biological indicators. Mar. Geol. 163, 353–365. https://doi.org/10.1016/S0025-3227(99)00117-6.

Baker, R.G.V., Haworth, R.J., 2000b. Smooth or oscillating late Holocene sea-level curve? Evidence from the palaeo-zoology of fixed biological indicators in East Australia and beyond. Mar. Geol. 163, 367–386. https://doi.org/10.1016/S0025-3227(99)00118-8.

Bard, E., Arnold, M., Mangerud, J., Paterne, M., Labeyrie, L., Duprat, J., Mélières, M.A., Sønstegaard, E., Duplessy, J.C., 1994. The North Atlantic atmosphere-sea surface 14C gradient during the Younger Dryas climatic event. Earth Planet. Sci. Lett. 126, 275–287. https://doi.org/10.1016/0012-821X(94)90112-0.

Bard, E., Arnold, M., Hamelin, B., Tisnerat-Laborde, N., Cabioch, G., 1998. Radiocarbon calibration by means of mass spectrometric $^{230}Th/^{234}U$ and ^{14}C ages of corals: an updated database including samples from Barbados, Mururoa and Tahiti. Radiocarbon 40, 1085–1092. https://doi.org/10.1017/S0033822200019135.

Bender, M., Mann, T., Stocchi, P., Kneer, D., Schöne, T., Illigner, J., Jompa, J., Rovere, A., 2020. Late Holocene (0–6 ka) sea-level changes in the Makassar Strait, Indonesia. Clim. Past 16, 1187–1205. https://doi.org/10.5194/cp-16-1187-2020.

Bird, M.I., Austin, W.E.N., Wurster, C.M., Fifield, L.K., Mojtahid, M., Sargeant, C., 2010. Punctuated eustatic sea-level rise in the early mid-Holocene. Geology 38, 803–806. https://doi.org/10.1130/G31066.1.

Bolton, A., Goodkin, N.F., Druffel, E.R.M., Griffin, S., Murty, S.A., 2016. Upwelling of Pacific intermediate water in the South China Sea revealed by coral radiocarbon record. Radiocarbon 58, 37–53. https://doi.org/10.1017/RDC.2015.4.

Bradley, S.L., Milne, G.A., Horton, B.P., Zong, Y., 2016. Modelling Sea level data from China and Malay-Thailand to estimate Holocene ice-volume equivalent sea level change. Quat. Sci. Rev. 137, 54–68. https://doi.org/10.1016/j.quascirev.2016.02.002.

Broecker, W.S., Denton, G.H., Edwards, R.L., Cheng, H., Alley, R.B., Putnam, A.E., 2010. Putting the Younger Dryas cold event into context. Quat. Sci. Rev. 29, 1078–1081. https://doi.org/10.1016/j.quascirev.2010.02.019.

Bronk Ramsey, C., 2009. Bayesian analysis of radiocarbon dates. Radiocarbon 51, 337–360. https://doi.org/10.1017/S0033822200033865.

Cao, L., Fairbanks, R.G., Mortlock, R.A., Risk, M.J., 2007. Radiocarbon reservoir age of high latitude North Atlantic surface water during the last deglacial. Quat. Sci. Rev. 26, 732–742. https://doi.org/10.1016/j.quascirev.2006.10.001.

Cheng, H., Edwards, R.L., Shen, C.-C., Polyak, V.J., Asmerom, Y., Woodhead, J., Hellstrom, J., Wang, Y., Kong, X., Spötl, C., Wang, X., Alexander, E.C., 2013. Improvements in ^{230}Th dating, ^{230}Th and ^{234}U half-life values, and U–Th isotopic measurements by multi-collector inductively coupled plasma mass spectrometry. Earth Planet. Sci. Lett. 371, 82–91. https://doi.org/10.1016/j.epsl.2013.04.006.

Chiang, H.-W., Lu, Y., Wang, X., Lin, K., Liu, X., 2019. Optimizing MC-ICP-MS with SEM protocols for determination of U and Th isotope ratios and ^{230}Th ages in carbonates.

Quat. Geochronol. 50, 75–90. https://doi.org/10.1016/j.quageo.2018.10.003.
Cutler, K.B., Gray, S.C., Burr, G.S., Edwards, R.L., Taylor, F.W., Cabioch, G., Beck, J.W., Cheng, H., Moore, J., 2004. Radiocarbon calibration and comparison to 50 kyr BP with paired ^{14}C and ^{230}Th dating of corals from Vanuatu and Papua New Guinea. Radiocarbon 46, 1127–1160. https://doi.org/10.1017/S0033822200033063.
Dang, P.X., Mitsuguchi, T., Kitagawa, H., Shibata, Y., Kobayashi, T., 2004. Marine reservoir correction in the south of Vietnam estimated from an annually-banded coral. Radiocarbon 46, 657–660. https://doi.org/10.1017/S0033822200035712.
de Klerk, L.G., 1982. Zeespiegels, riffen en kustvlakten in zuidwest Sulawesi, Indonesië: een morfogenetisch-bodemkundige studie. PhD thesis. Geografisch Instituut, Rijksuniversiteit te Utrecht. https://library.wur.nl/WebQuery/file/isric/fulltext/isricu_i26244_001.pdf.
Dutton, A., Carlson, A.E., Long, A.J., Milne, G.A., Clark, P.U., DeConto, R., Horton, B.P., Rahmstorf, S., Raymo, M.E., 2015. Sea-level rise due to polar ice-sheet mass loss during past warm periods. Science 349https://doi.org/10.1126/science.aaa4019. aaa4019.
Edwards, R.L., Chen, J.H., Wasserburg, G.J., 1987. ^{238}U-^{234}U-^{230}Th-^{232}Th systematics and the precise measurement of time over the past 500,000 years. Earth Planet. Sci. Lett. 81, 175–192. https://doi.org/10.1016/0012-821X(87)90154-3.
Egbert, G.D., Erofeeva, S.Y., 2002. Efficient inverse modeling of barotropic ocean tides. J. Atmos. Ocean. Technol. 19, 183–204. https://doi.org/10.1175/1520-0426(2002)019%3C0183:EIMOBO%3E2.0.CO;2.
Geyh, M.A., Kudrass, H.-R., Streif, H., 1979. Sea-level changes during the late Pleistocene and Holocene in the Strait of Malacca. Nature 278, 441–443. https://doi.org/10.1038/278441a0.
Heaton, T.J., Köhler, P., Butzin, M., Bard, E., Reimer, R.W., Austin, W.E., Ramsey, C.B., Grootes, P.M., Hughen, K.A., Kromer, B., Reimer, P.J., 2020. Marine20—the marine radiocarbon age calibration curve (0–55,000 cal BP). Radiocarbon 62, 779–820. https://doi.org/10.1017/RDC.2020.68.
Hibbert, F.D., Rohling, E.J., Dutton, A., Williams, F.H., Chutcharavan, P.M., Zhao, C., Tamisiea, M.E., 2016. Coral indicators of past sea-level change: a global repository of U-series dated benchmarks. Quat. Sci. Rev. 145, 1–56. https://doi.org/10.1016/j.quascirev.2016.04.019.
Horton, B.P., Edwards, R.J., Lloyd, J.M., 2000. Implications of a microfossil-based transfer function in Holocene sea-level studies. Geol. Soc. Lond., Spec. Publ. 166, 41–54. https://doi.org/10.1144/GSL.SP.2000.166.01.03.
Horton, B.P., Gibbard, P.L., Milne, G.M., Morley, R.J., Purintavaragul, C., Stargardt, J.M., 2005. Holocene Sea levels and palaeoenvironments, Malay-Thai Peninsula, Southeast Asia. The Holocene 15, 1199–1213. https://doi.org/10.1191/0959683605hl891rp.
Horton, B.P., Kopp, R.E., Garner, A.J., Hay, C.C., Khan, N.S., Roy, K., Shaw, T.A., 2018. Mapping sea-level change in time, space, and probability. Annu. Rev. Environ. Resour. 43, 481–521. https://doi.org/10.1146/annurev-environ-102017-025826.
Hughen, K.A., Baillie, M.G.L., Bard, E., Warren Beck, J., Bertrand, C.J.H., Blackwell, P.G., Buck, C.E., Burr, G.S., Cutler, K.B., Damon, P.E., Edwards, R.L., Fairbanks, R.G., Friedrich, M., Guilderson, T.P., Kromer, B., McCormac, G., Manning, S., Bronk Ramsey, C., Reimer, P.J., Reimer, R.W., Remmele, S., Southon, J.R., Stuiver, M., Talamo, S., Taylor, F.W., van der Plicht, J., Weyhenmeyer, C.E., 2004. Marine04 marine radiocarbon age calibration, 0–26 cal kyr BP. Radiocarbon 46, 1059–1086. https://doi.org/10.1017/S0033822200033002.
Jaffey, A.H., Flynn, K.F., Glendenin, L.E., Bentley, W.C., Essling, A.M., 1971. Precision measurement of half-lives and specific activities of ^{235}U and ^{238}U. Phys. Rev C 4, 1889. https://doi.org/10.1103/PhysRevC.4.1889.
Kamaludin, B.H., 2003. Mid-Holocene to recent sea level changes in Peninsular Malaysia: a tectonic implication. Geol. Soc. Malaysia Bull. 46, 313–318. https://doi.org/10.7186/bgsm46200352.
Kench, P.S., McLean, R.F., Owen, S.D., Ryan, E., Morgan, K.M., Ke, L., Wang, X., Roy, K., 2020. Climate-forced sea-level lowstands in the Indian Ocean during the last two millennia. Nat. Geosci. 13, 61–64. https://doi.org/10.1038/s41561-019-0503-7.
Khan, N.S., Ashe, E., Shaw, T.A., Vacchi, M., Walker, J., Peltier, W.R., Kopp, R.E., Horton, B.P., 2015. Holocene relative sea-level changes from near-, intermediate-, and far-field locations. Curr. Clim. Change Rep. 1, 247–262. https://doi.org/10.1007/s40641-015-0029-z.
Khan, N.S., Horton, B.P., Engelhart, S., Rovere, A., Vacchi, M., Ashe, E.L., Törnqvist, T.E., Dutton, A., Hijma, M.P., Shennan, I., 2019. Inception of a global atlas of sea levels since the Last Glacial Maximum. Quat. Sci. Rev. 220, 359–371. https://doi.org/10.1016/j.quascirev.2019.07.016.
Lambeck, K., Rouby, H., Purcell, A., Sun, Y., Sambridge, M., 2014. Sea level and global ice volumes from the Last Glacial Maximum to the Holocene. Proc. Natl. Acad. Sci. 111, 15296–15303. https://doi.org/10.1073/pnas.1411762111.
Leonard, N.D., Zhao, J., Welsh, K.J., Feng, Y.-X., Smithers, S.G., Pandolfi, J.M., Clark, T.R., 2016. Holocene Sea level instability in the southern Great Barrier Reef, Australia: high-precision U–Th dating of fossil microatolls. Coral Reefs 35, 625–639. https://doi.org/10.1007/s00338-015-1384-x.
Lewis, S.E., Sloss, C.R., Murray-Wallace, C.V., Woodroffe, C.D., Smithers, S.G., 2013. Post-glacial sea-level changes around the Australian margin: a review. Quat. Sci. Rev. 74, 115–138. https://doi.org/10.1016/j.quascirev.2012.09.006.
Majewski, J.M., Switzer, A.D., Meltzner, A.J., Parham, P.R., Horton, B.P., Bradley, S.L., Pile, J., Chiang, H.-W., Wang, X., Ng, C.T., Tanzil, J., Müller, M., Mujahid, A., 2018. Holocene relative sea-level records from coral microatolls in Western Borneo, South China Sea. The Holocene 28, 1431–1442. https://doi.org/10.1177/0959683618777061.
Mann, T., Rovere, A., Schöne, T., Klicpera, A., Stocchi, P., Lukman, M., Westphal, H., 2016. The magnitude of a mid-Holocene sea-level highstand in the Strait of Makassar. Geomorphology 257, 155–163. https://doi.org/10.1016/j.geomorph.2015.12.023.
Mann, T., Bender, M., Lorscheid, T., Stocchi, P., Vacchi, M., Switzer, A.D., Rovere, A., 2019. Holocene Sea levels in Southeast Asia, Maldives, India and Sri Lanka: the SEAMIS database. Quat. Sci. Rev. 219, 112–125. https://doi.org/10.1016/j.quascirev.2019.07.007.
Martin, S.S., Wang, Y., Muzli, M., Wei, S., 2020. The 1922 Peninsula Malaysia Earthquakes: rare intraplate seismicity within the Sundaland Block in Southeast Asia. Seismol. Res. Lett. 91, 2531–2545. https://doi.org/10.1785/0220200052.
McGregor, H.V., Gagan, M.K., McCulloch, M.T., Hodge, E., Mortimer, G., 2008. Mid-Holocene variability in the marine ^{14}C reservoir age for northern coastal Papua New Guinea. Quat. Geochronol. 3, 213–225. https://doi.org/10.1016/j.quageo.2007.11.002.
Meltzner, A.J., Woodroffe, C.D., 2015. Coral microatolls. In: Shennan, I., Long, A.J., Horton, B.P. (Eds.), Handbook of Sea-Level Research. John Wiley & Sons, Ltd., Chichester, UK, pp. 125–145. https://doi.org/10.1002/9781118452547.ch8.
Meltzner, A.J., Sieh, K., Chiang, H.-W., Shen, C.-C., Suwargadi, B.W., Natawidjaja, D.H., Philibosian, B.E., Briggs, R.W., Galetzka, J., 2010. Coral evidence for earthquake recurrence and an AD 1390–1455 cluster at the south end of the 2004 Aceh–Andaman rupture. J. Geophys. Res. 115, B10402. https://doi.org/10.1029/2010JB007499.
Meltzner, A.J., Switzer, A.D., Horton, B.P., Ashe, E., Qiu, Q., Hill, D.F., Bradley, S.L., Kopp, R.E., Hill, E.M., Majewski, J.M., Natawidjaja, D.H., Suwargadi, B.W., 2017. Half-metre sea-level fluctuations on centennial timescales from mid-Holocene corals of Southeast Asia. Nat. Commun. 8, 14387. https://doi.org/10.1038/ncomms14387.
Milne, G.A., Gehrels, W.R., Hughes, C.W., Tamisiea, M.E., 2009. Identifying the causes of sea-level change. Nat. Geosci. 2, 471–478. https://doi.org/10.1038/ngeo544.
Mitrovica, J.X., Milne, G.A., 2002. On the origin of late Holocene sea-level highstands within equatorial ocean basins. Quat. Sci. Rev. 21, 2179–2190. https://doi.org/10.1016/S0277-3791(02)00080-X.
Nakada, M., Lambeck, K., 1989. Late Pleistocene and Holocene sea-level change in the Australian region and mantle rheology. Geophys. J. Int. 96, 497–517. https://doi.org/10.1111/j.1365-246X.1989.tb06010.x.
Parham, P.R., 2016. Late Cenozoic relative sea-level highstand record from Peninsular Malaysia and Malaysian Borneo: Implications for vertical crustal movements. Bull. Geol. Soc. Malaysia 62, 91–115. https://doi.org/10.7186/bgsm62201612.
Parham, P.R., 2019. Subsiding Sundaland: comment. Geology 47, e469. https://doi.org/10.1130/G46294C.1.
Parham, P.R., Saito, Y., Sapon, N., Suriadi, R., Mohtar, N.A., 2014. Evidence for ca. 7-ka maximum Holocene transgression on the Peninsular Malaysia east coast. J. Quat. Sci. 29, 414–422. https://doi.org/10.1002/jqs.2714.
Peltier, W.R., 1996. Mantle viscosity and ice-age ice sheet topography. Science 273, 1359–1364. https://doi.org/10.1126/science.273.5280.1359.
Peltier, W.R., 2004. Global glacial isostasy and the surface of the ice-age Earth: the ICE-5G (VM2) model and GRACE. Annu. Rev. Earth Planet. Sci. 32, 111–149. https://doi.org/10.1146/annurev.earth.32.082503.144359.
Peltier, W.R., Argus, D.F., Drummond, R., 2015. Space geodesy constrains ice age terminal deglaciation: the global ICE-6G_C (VM5a) model. J. Geophys. Res. 120, 450–487. https://doi.org/10.1002/2014JB011176.
Perry, C.T., Smithers, S.G., 2011. Cycles of coral reef 'turn-on', rapid growth and 'turn-off' over the past 8500 years: a context for understanding modern ecological states and trajectories. Glob. Chang. Biol. 17, 76–86. https://doi.org/10.1111/j.1365-2486.2010.02181.x.
Petchey, F., Clark, G., 2011. Tongatapu hardwater: investigation into the ^{14}C marine reservoir offset in lagoon, reef and open ocean environments of a limestone island. Quat. Geochronol. 6, 539–549. https://doi.org/10.1016/j.quageo.2011.08.001.
Petchey, F., Allen, M.S., Addison, D.J., Anderson, A., 2009. Stability in the South Pacific surface marine ^{14}C reservoir over the last 750 years. Evidence from American Samoa, the southern Cook Islands and the Marquesas. J. Archaeol. Sci. 36, 2234–2243. https://doi.org/10.1016/j.jas.2009.06.008.
Philibosian, B., Sieh, K., Avouac, J.P., Natawidjaja, D.H., Chiang, H.W., Wu, C.C., Perfettini, H., Shen, C.C., Daryono, M.R., Suwargadi, B.W., 2014. Rupture and variable coupling behavior of the Mentawai segment of the Sunda megathrust during the supercycle culmination of 1797 to 1833. J. Geophys. Res. 119, 7258–7287. https://doi.org/10.1002/2014JB011200.
Reimer, R.W., Reimer, P.J., 2017. An online application for ΔR calculation. Radiocarbon 59, 1623–1627. https://doi.org/10.1017/RDC.2016.117.
Reimer, P.J., Baillie, M.G., Bard, E., Bayliss, A., Beck, J.W., Blackwell, P.G., Ramsey, C.B., Buck, C.E., Burr, G.S., Edwards, R.L., Friedrich, M., 2009. IntCal09 and Marine09 radiocarbon age calibration curves, 0–50,000 years cal BP. Radiocarbon 51, 1111–1150. https://doi.org/10.1017/S0033822200034202.
Reimer, P.J., Bard, E., Bayliss, A., Beck, J.W., Blackwell, P.G., Ramsey, C.B., Buck, C.E., Cheng, H., Edwards, R.L., Friedrich, M., Grootes, P.M., Guilderson, T.P., Haflidason, H., Hajdas, I., Hatté, C., Heaton, T.J., Hoffmann, D.L., Hogg, A.G., Hughen, K.A., Kaiser, K.F., Kromer, B., Manning, S.W., Niu, M., Reimer, R.W., Richards, D.A., Scott, E.M., Southon, J.R., Staff, R.A, Turney, C.S.M., van der Plicht, J., 2013a. IntCal13 and Marine13 radiocarbon age calibration curves 0–50,000 years cal BP. Radiocarbon 55, 1869–1887. https://doi.org/10.2458/azu_js_rc.55.16947.
Reimer, P.J., Bard, E., Bayliss, A., Beck, J.W., Blackwell, P.G., Ramsey, C.B., Brown, D.M., Buck, C.E., Edwards, R.L., Friedrich, M., Grootes, P.M., Guilderson, T.P., Haflidason, H., Hajdas, I., Hatté, C., Heaton, T.J., Hogg, A.G., Hughen, K.A., Kaiser, K.F., Kromer, B., Manning, S.W., Reimer, R.W., Richards, D.A., Scott, E.M., Southon, J.R., Turney, C.S.M., van der Plicht, J., 2013b. Selection and treatment of data for radiocarbon calibration: an update to the international calibration (IntCal) criteria. Radiocarbon 55, 1923–1945. https://doi.org/10.2458/azu_js_rc.55.16955.
Russell, N., Cook, G.T., Ascough, P.L., Scott, E.M., Dugmore, A.J., 2011. Examining the inherent variability in ΔR: new methods of presenting ΔR values and implications for MRE studies. Radiocarbon 53, 277–288. https://doi.org/10.1017/S003382220005654X.
Ryan, E.J., Smithers, S.G., Lewis, S.E., Clark, T.R., Zhao, J.X., 2016. The influence of sea

level and cyclones on Holocene reef flat development: Middle Island, central Great Barrier Reef. Coral Reefs 35, 805–818. https://doi.org/10.1007/s00338-016-1453-9.
Sarr, A.C., Husson, L., Sepulchre, P., Pastier, A.M., Pedoja, K., Elliot, M., Arias-Ruiz, C., Solihuddin, T., Aribowo, S., 2019. Subsiding Sundaland. Geology 47, 119–122. https://doi.org/10.1130/G45629.1.
Scoffin, T.P., Stoddart, D.R., 1978. The nature and significance of microatolls. Phil. Trans. R. Soc. Lond. B 284, 99–122. https://doi.org/10.1098/rstb.1978.0055.
Shen, C.-C., Wu, C.-C., Cheng, H., Edwards, R.L., Hsieh, Y.-T., Gallet, S., Chang, C.-C., Li, T.-Y., Lam, D.D., Kano, A., Hori, M., Spotl, C., 2012. High-precision and high-resolution carbonate ^{230}Th dating by MC-ICP-MS with SEM protocols. Geochim. Cosmochim. Acta 99, 71–86. https://doi.org/10.1016/j.gca.2012.09.018.
Shennan, I., 1986. Flandrian sea-level changes in the Fenland. II: Tendencies of sea-level movement, altitudinal changes, and local and regional factors. J. Quat. Sci. 1, 155–179. https://doi.org/10.1002/jqs.3390010205.
Shennan, I., Horton, B., 2002. Holocene land- and sea-level changes in Great Britain. J. Quat. Sci. 17, 511–526. https://doi.org/10.1002/jqs.710.
Shennan, I., Long, A.J., Horton, B.P. (Eds.), 2015. Handbook of Sea-Level Research. John Wiley & Sons, Ltd., Chichester, UK. https://doi.org/10.1002/9781118452547.
Sieh, K., Natawidjaja, D.H., Meltzner, A.J., Shen, C.-C., Cheng, H., Li, K.-S., Suwargadi, B.W., Galetzka, J., Philibosian, B., Edwards, R.L., 2008. Earthquake supercycles inferred from sea-level changes recorded in the corals of West Sumatra. Science 322, 1674–1678. https://doi.org/10.1126/science.1163589.
Simons, W.J.F., Socquet, A., Vigny, C., Ambrosius, B.A.C., Haji Abu, S., Promthong, C., Subarya, C., Sarsito, D.A., Matheussen, S., Morgan, P., Spakman, W., 2007. A decade of GPS in Southeast Asia: resolving Sundaland motion and boundaries. J. Geophys. Res. 112, B06420. https://doi.org/10.1029/2005JB003868.
Sloss, C.R., Murray-Wallace, C.V., Jones, B.G., 2007. Holocene sea-level change on the southeast coast of Australia: a review. The Holocene 17, 999–1014. https://doi.org/10.1177/0959683607082415.
Smithers, S.G., Woodroffe, C.D., 2000. Microatolls as sea-level indicators on a mid-ocean atoll. Mar. Geol. 168, 61–78. https://doi.org/10.1016/S0025-3227(00)00043-8.
Soulet, G., 2015. Methods and codes for reservoir–atmosphere 14C age offset calculations. Quat. Geochronol. 29, 97–103. https://doi.org/10.1016/j.quageo.2015.05.023.
Southon, J., Kashgarian, M., Fontugne, M., Metivier, B., Yim, W.W.-S., 2002. Marine reservoir corrections for the Indian Ocean and Southeast Asia. Radiocarbon 44, 167–180. https://doi.org/10.1017/S0033822200064778.
Stattegger, K., Tjallingii, R., Saito, Y., Michelli, M., Thanh, N.T., Wetzel, A., 2013. Mid to late Holocene sea-level reconstruction of Southeast Vietnam using beachrock and beach-ridge deposits. Glob. Planet. Chang. 110, 214–222. https://doi.org/10.1016/j.gloplacha.2013.08.014.
Staubwasser, M., Sirocko, F., Grootes, P.M., Erlenkeuser, H., 2002. South Asian monsoon climate change and radiocarbon in the Arabian Sea during early and middle Holocene. Paleoceanography 17, 1063. https://doi.org/10.1029/2000PA000608.
Stuiver, M., Polach, H.A., 1977. Discussion: reporting of ^{14}C data. Radiocarbon 19, 355–363. https://doi.org/10.1017/S0033822200003672.
Stuiver, M., Pearson, G.W., Braziunas, T., 1986. Radiocarbon age calibration of marine samples back to 9000 cal yr BP. Radiocarbon 28, 980–1021. https://doi.org/10.1017/S0033822200060264.
Tam, C.-Y., Zong, Y., Kamaludin, B.H., Hamlee, B.I., Habibah, B.J., Xiong, H., Wu, P., Sun, Y., Huang, G., Zheng, Z., 2018. A below-the-present late Holocene relative sea level and the glacial isostatic adjustment during the Holocene in the Malay Peninsula. Quat. Sci. Rev. 201, 206–222. https://doi.org/10.1016/j.quascirev.2018.10.009.
Tjia, H.D., Fujii, S., Kigoshi, K., Sugimura, A., Zakaria, T., 1972. Radiocarbon dates of elevated shorelines, Indonesia and Malaysia. Part 1. Quat. Res. 2, 487–495. https://doi.org/10.1016/0033-5894(72)90087-7.
Turnbull, J., Zondervan, A., Kaiser, J., Norris, M., Dahl, J., Baisden, T., Lehman, S., 2015. High-Precision Atmospheric 14CO2 Measurement at the Rafter Radiocarbon Laboratory. Radiocarbon 57, 377–388. https://doi.org/10.2458/azu_rc.57.18390.
van de Plassche, O., 1986. Introduction. In: van de Plassche, O. (Ed.), Sea-Level Research: A Manual for the Collection and Evaluation of Data. Geo Books, Norwich, UK, pp. 1–26. https://doi.org/10.1007/978-94-009-4215-8_1.
Wirojudo, G.K., Wongsosantiko, A., 1985. Tertiary tectonic evolution and related hydrocarbon potential in the Natuna area. Energy 10, 433–455. https://doi.org/10.1016/0360-5442(85)90059-3.
Woodroffe, S.A., Barlow, N.L.M., 2015. Reference water level and tidal datum. In: Shennan, I., Long, A.J., Horton, B.P. (Eds.), Handbook of Sea-Level Research. John Wiley & Sons, Ltd., Chichester, UK, pp. 171–180. https://doi.org/10.1002/9781118452547.ch11.
Woodroffe, S.A., Horton, B.P., 2005. Holocene sea-level changes in the Indo-Pacific. J. Asian Earth Sci. 25, 29–43. https://doi.org/10.1016/j.jseaes.2004.01.009.
Woodroffe, C.D., Murray-Wallace, C.V., 2012. Sea-level rise and coastal change: the past as a guide to the future. Quat. Sci. Rev. 54, 4–11. https://doi.org/10.1016/j.quascirev.2012.05.009.
Yu, K.-F., Zhao, J.-X., Done, T., Chen, T.-G., 2009. Microatoll record for large century-scale sea-level fluctuations in the mid-Holocene. Quat. Res. 71, 354–360. https://doi.org/10.1016/j.yqres.2009.02.003.
Yu, K., Hua, Q., Zhao, J.-X., Hodge, E., Fink, D., Barbetti, M., 2010. Holocene marine ^{14}C reservoir age variability: evidence from ^{230}Th-dated corals in the South China Sea. Paleoceanography 25, PA3205. https://doi.org/10.1029/2009PA001831.
Zondervan, A., Hauser, T.M., Kaiser, J., Kitchen, R.L., Turnbull, J.C., West, J.G., 2015. XCAMS: the compact ^{14}C accelerator mass spectrometer extended for ^{10}Be and ^{26}Al at GNS Science, New Zealand. Nucl. Instrum. Methods Phys. Res., Sect. B 361, 25–33. https://doi.org/10.1016/j.nimb.2015.03.013.
Zong, Y., 2004. Mid-Holocene sea-level highstand along the southeast coast of China. Quat. Int. 117, 55–67. https://doi.org/10.1016/S1040-6182(03)00116-2.

Update

Marine Geology

Volume 432, Issue , February 2021, Page

DOI: https://doi.org/10.1016/j.margeo.2020.106399

Contents lists available at ScienceDirect

Marine Geology

journal homepage: www.elsevier.com/locate/margo

Corrigendum

Corrigendum to "Relative sea-level stability and the radiocarbon marine reservoir correction at Natuna Island, Indonesia, since 6400 yr BP" [Marine Geology 430 (2020) 106342]

Jeannette Xiu Wen Wan [a,b,c,f,*], Aron J. Meltzner [a,b,*], Adam D. Switzer [a,b], Ke Lin [a], Xianfeng Wang [a,b], Sarah L. Bradley [d], Danny H. Natawidjaja [e], Bambang W. Suwargadi [e], Benjamin P. Horton [a,b]

[a] Earth Observatory of Singapore, Nanyang Technological University, 50 Nanyang Avenue, Singapore 639798, Singapore
[b] Asian School of the Environment, Nanyang Technological University, 50 Nanyang Avenue, Singapore 639798, Singapore
[c] CN Yang Scholars Programme, Nanyang Technological University, 50 Nanyang Avenue, Singapore 639798, Singapore
[d] Department of Geography, The University of Sheffield, Winter Street, Sheffield S3 7ND, United Kingdom
[e] Research Center for Geotechnology, Indonesian Institute of Sciences (LIPI), Kompleks LIPI, Gedung 70, Jalan Sangkuriang, Bandung, Jawa Barat 40135, Indonesia
[f] Department of Earth and Planetary Sciences, McGill University, 3450 University Street, Montreal, Quebec H3A 0E8, Canada

The authors regret that the uncertainties stated in our paper for the overall estimates of the Marine20 ΔR (the radiocarbon marine reservoir correction) across all Natuna Island sites, using *deltar* and OxCal, were incorrect.

The incorrect values provided in the last row of Table A2 for the overall ΔR for PNTN for Marine20 were −143 ± 176 yr from the program *deltar* and −145 ± 173 yr from OxCal. Instead, the correct values for these quantities are −143 ± 62 yr from *deltar* and −145 ± 48 yr from OxCal.

Notably, the true uncertainties for those quantities were lower than we had stated in the paper. Considering the corrected values, the Marine20 ΔR uncertainties and the Marine13 ΔR uncertainties are of similar magnitudes.

In addition to the two mistakes mentioned above in Table A2, the incorrect uncertainties were plotted on Fig. 4b, and they were stated five times in the text of the article (in the abstract, §1, §4.1, §5.1, §6). They were also stated incorrectly in the paper's highlights section.

Below we include an updated version of Table A2 and Fig. 4b.

None of our other conclusions are affected.

The authors would like to apologise for any inconvenience caused.

Table A2
Comparison of ΔR estimates based on *deltar* and OxCal.

Sample ID[a]	ΔR (yr) ± 1σ for Marine13		ΔR (yr) ± 1σ for Marine2	
	from *deltar*[a]	from OxCal[b]	from *deltar*[a]	from OxCal[b]
PNTN-A-F1	−16 ± 15	−15 ± 27	−165 ± 31	−164 ± 4
PNTN-A-F2	172 ± 12	173 ± 31	−19 ± 23	−18 ± 54
PNTN-A-F3	−38 ± 10	−39 ± 28	−210 ± 21	−212 ± 5
PNTN-A-F4A	10 ± 32	7 ± 35	−183 ± 64	−191 ± 5
PNTN-A-F4B	−20 ± 12	−20 ± 28	−206 ± 24	−206 ± 5
PNTN-B-F1	22 ± 8	23 ± 26	−118 ± 17	−118 ± 4
PNTN-B-F2	18 ± 38	20 ± 27	−144 ± 77	−142 ± 4
PNTN-B-F3	−10 ± 10	−10 ± 26	−161 ± 23	−160 ± 4
PNTN-C-F1	36 ± 40	31 ± 31	−96 ± 79	−107 ± 4
PNTN-C-F2	20 ± 20	22 ± 27	−128 ± 40	−125 ± 4
PNTN-D-F1	−3 ± 23	−6 ± 31	−144 ± 45	−149 ± 4
PNTN-D-F2	2 ± 36	4 ± 27	−155 ± 74	−153 ± 4
Joint[c] ΔR for PNTN		15 ± 9		−145 ± 1
Overall[d] ΔR for PNTN	15 ± 63	14 ± 51	−143 ± 62	−145 ± 4

[a] Values as in Table 4.
[b] ΔR estimates from the OxCal program (Bronk Ramsey, 2009) are base Bayesian methodologies. Details are in Appendix C and Supplementary Tex
[c] The joint ΔR is determined from the OxCal scripts in the Supplementary T and is a single value of ΔR that best fits all the age data from the PNTN sit
[d] The overall ΔR is calculated according to Eqs. 1 and 3, and captures variance in ΔR in the data set.

DOI of original article: https://doi.org/10.1016/j.margeo.2020.106342.
* Corresponding authors at: Earth Observatory of Singapore, Nanyang Technological University, 50 Nanyang Avenue, Singapore 639798, Singapore.
E-mail addresses: jwan007@ntu.edu.sg (J.X.W. Wan), meltzner@ntu.edu.sg (A.J. Meltzner).

https://doi.org/10.1016/j.margeo.2020.106399

Available online 23 December 2020
0025-3227/© 2020 The Author(s). Published by Elsevier B.V. All rights reserved.

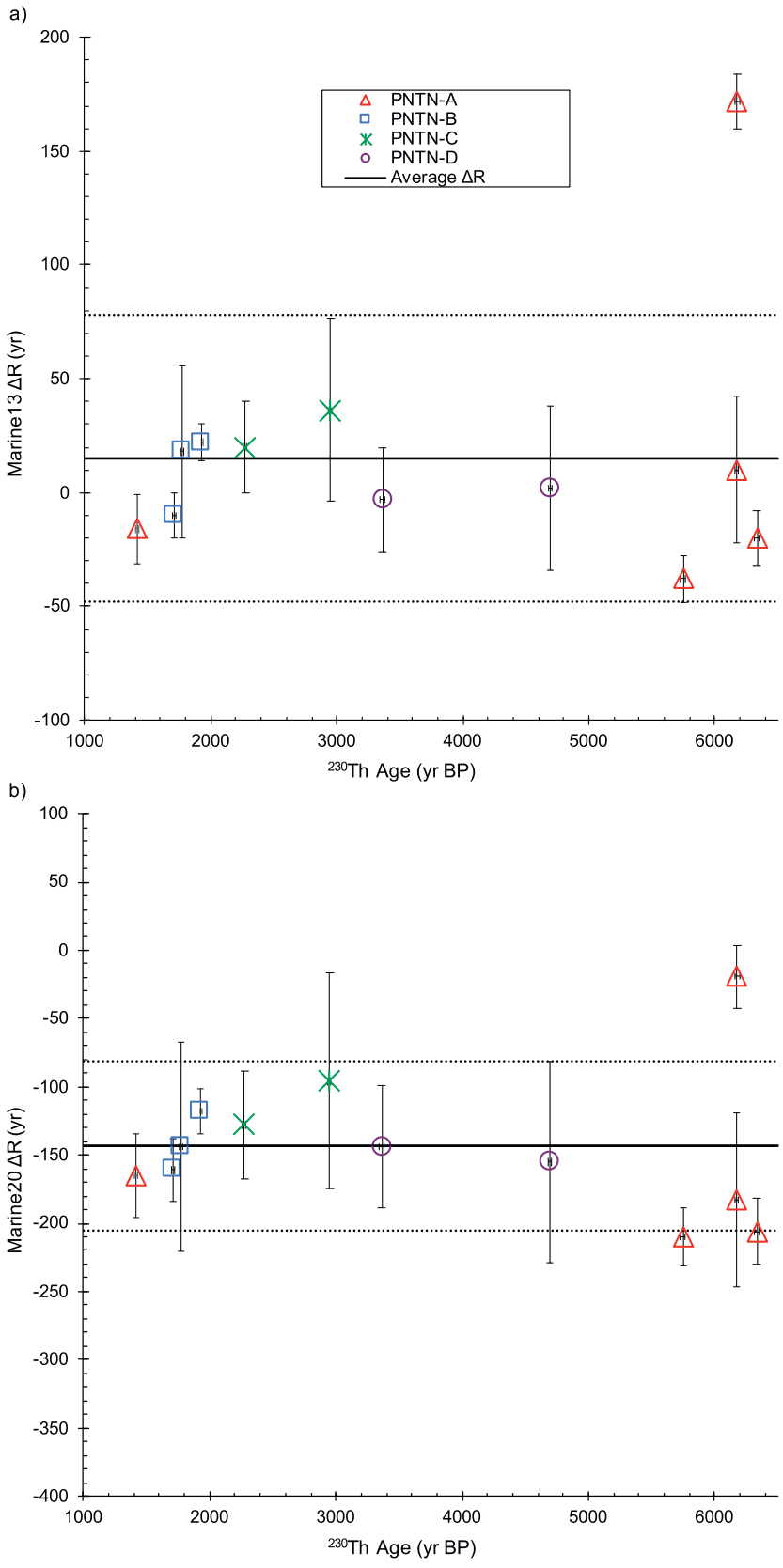

Fig. 4. ΔR over time obtained from paired ^{14}C and ^{230}Th ages of *Porites* coral samples from Natuna Island using a) Marine13, and b) Marine20 marine radioca age calibration curves on *deltar*. Horizontal errors represent experimental uncertainty of ^{230}Th ages to 2σ; vertical errors (ΔR) are 1σ. Solid and dashed horizo lines denote the weighted average of ΔR from all samples, plus or minus one weighted standard deviation.